Petroleum Science 21 (2024) 2218–2239

Contents lists available at ScienceDirect

Petroleum Science

journal homepage: www.keaipublishing.com/en/journals/petroleum-science

Original Paper

Prediction and quantification of effective gas source rocks in a lacustrine basin: Western Depression in the Liaohe Subbasin, China

Si-Bo Yang [a], Mei-Jun Li [a, b, *], Hong Xiao [a], Fang-Zheng Wang [a], Guo-Gang Cai [c], Shuang-Quan Huang [c]

[a] State Key Laboratory of Petroleum Resources and Prospecting, College of Geosciences, China University of Petroleum, Beijing, 102249, China
[b] China University of Petroleum-Beijing at Karamay, College of Petroleum, Karamay, Xinjiang, 834000, China
[c] Research Institute of Petroleum Exploration and Development, Liaohe Oilfield Company, PetroChina, Panjin, 124010, Liaoning, China

ARTICLE INFO

Article history:
Received 19 May 2023
Received in revised form
26 July 2023
Accepted 13 March 2024
Available online 15 March 2024

Edited by Jie Hao and Teng Zhu

Keywords:
Effective gas source rock
3D geological modeling
Spatial distribution
Geochemical characteristics
Lacustrine rift basin

ABSTRACT

Due to limited data on the geochemical properties of natural gas, estimations are needed for the effective gas source rock in evaluating gas potential. However, the pronounced heterogeneity of mudstones in lacustrine successions complicates the prediction of the presence and geochemical characteristics of gas source rocks. In this paper, the Liaohe Subbasin of Northeast China is used as an example to construct a practical methodology for locating effective gas source rocks in typical lacustrine basins. Three types of gas source rocks, microbial, oil-type, and coal-type, were distinguished according to the different genetic types of their natural gas. A practical three-dimensional geological model was developed, refined, and applied to determine the spatial distribution of the mudstones in the Western Depression of the Liaohe Subbasin and to describe the geochemical characteristics (the abundance, type, and maturation levels of the organic matter). Application of the model in the subbasin indicates that the sedimentary facies have led to heterogeneity in the mudstones, particularly with respect to organic matter types. The effective gas source rock model constructed for the Western Depression shows that the upper sequence (SQ2) of the Fourth member (Mbr 4) of the Eocene Shahejie Formation (Fm) and the lower and middle sequences (SQ3 and SQ4) of the Third member (Mbr 3) form the principal gas-generating interval. The total volume of effective gas source rocks is estimated to be 586 km^3. The effective microbial, oil-type, and coal-type gas source rocks are primarily found in the shallow western slope, the central sags, and the eastern slope of the Western Depression, respectively. This study provides a practical approach for more accurately identifying the occurrence and geochemical characteristics of effective natural gas source rocks, enabling a precise quantitative estimation of natural gas reserves.

1. Introduction

Most rift lacustrine basins, such as Bohai Bay Basin in eastern China, are petroliferous basins with few large-scale gas pools (Qi and Yang, 2010; Xu et al., 2019; W.Y. Wang et al., 2022). Two main factors contribute to this: firstly, the dominant source rocks contain oil-prone kerogens of moderate maturity; secondly, multiple phases of tectonic activity have significantly weakened the sealing capacity of the cap layers (Dai et al., 1998; Lai, 2000). However, more and more gas pools with considerable reserves have been discovered in recent years, such as the Bozhong 19-6 in the Bozhong Depression, which strongly suggests that the natural gas resource potential in rift lacustrine basins has been underestimated (Hu et al., 2001; Xu et al., 2019; Wang et al., 2021).

In contrast to oil, natural gas can be generated at various thermal maturation stages of organic matter, including microbial and thermogenic phases. It can also be produced by the cracking of reservoir oils and, in some cases, even through abiogenic processes. This diversity in natural gas origins underscores the complexity of its formation and the varied conditions under which it can occur (Faramawy et al., 2016; Speight, 2022). Biogenic natural gas can be subdivided into microbial, coal-type, and oil-type by comparing their chemical, stable carbon, and hydrogen isotope compositions

* Corresponding author. State Key Laboratory of Petroleum Resources and Prospecting, College of Geosciences, China University of Petroleum, Beijing, 102249, China.
E-mail address: meijunli@cup.edu.cn (M.-J. Li).

https://doi.org/10.1016/j.petsci.2024.03.007

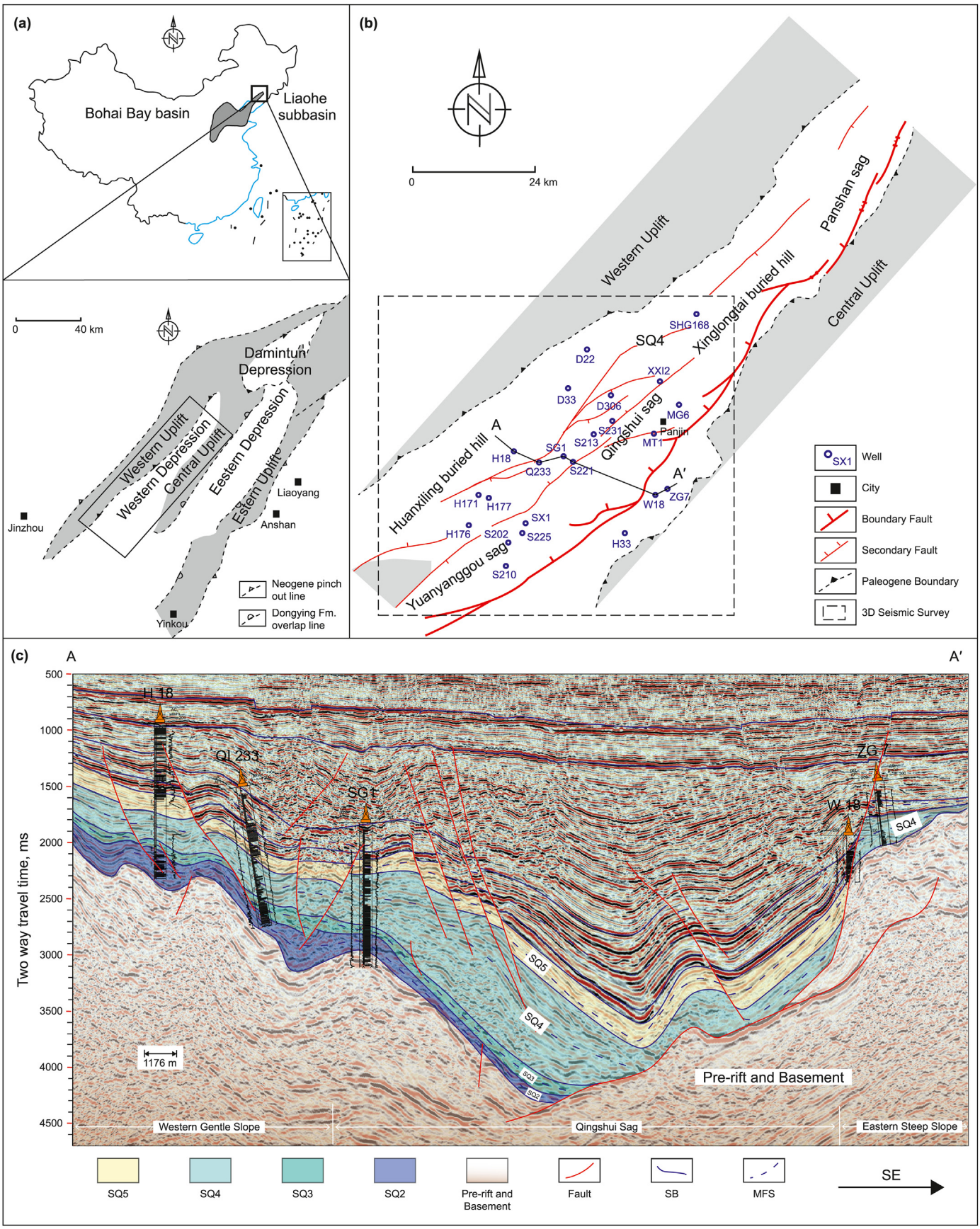

Fig. 1. (a) Location and structural subdivision of the Liaohe Subbasin; (modified after Li X., 2020). (b) Tectonic units of Western Depression, including main profiles A-A′ and important wells. (c) Cross section (profile A-A′) showing sequence stratigraphy in the study area; SQ2: sequence corresponding to upper Mbr 4 of the Shahejie Fm; SQ3: sequence corresponding to lower Mbr 3 of the Shahejie Fm; SQ4: sequence corresponding to middle Mbr 3 of the Shahejie Fm; SQ5: sequence corresponding to upper Mbr 3 of the Shahejie Fm; SB: Sequence Boundary; MFS: Maximum Flood Surface.

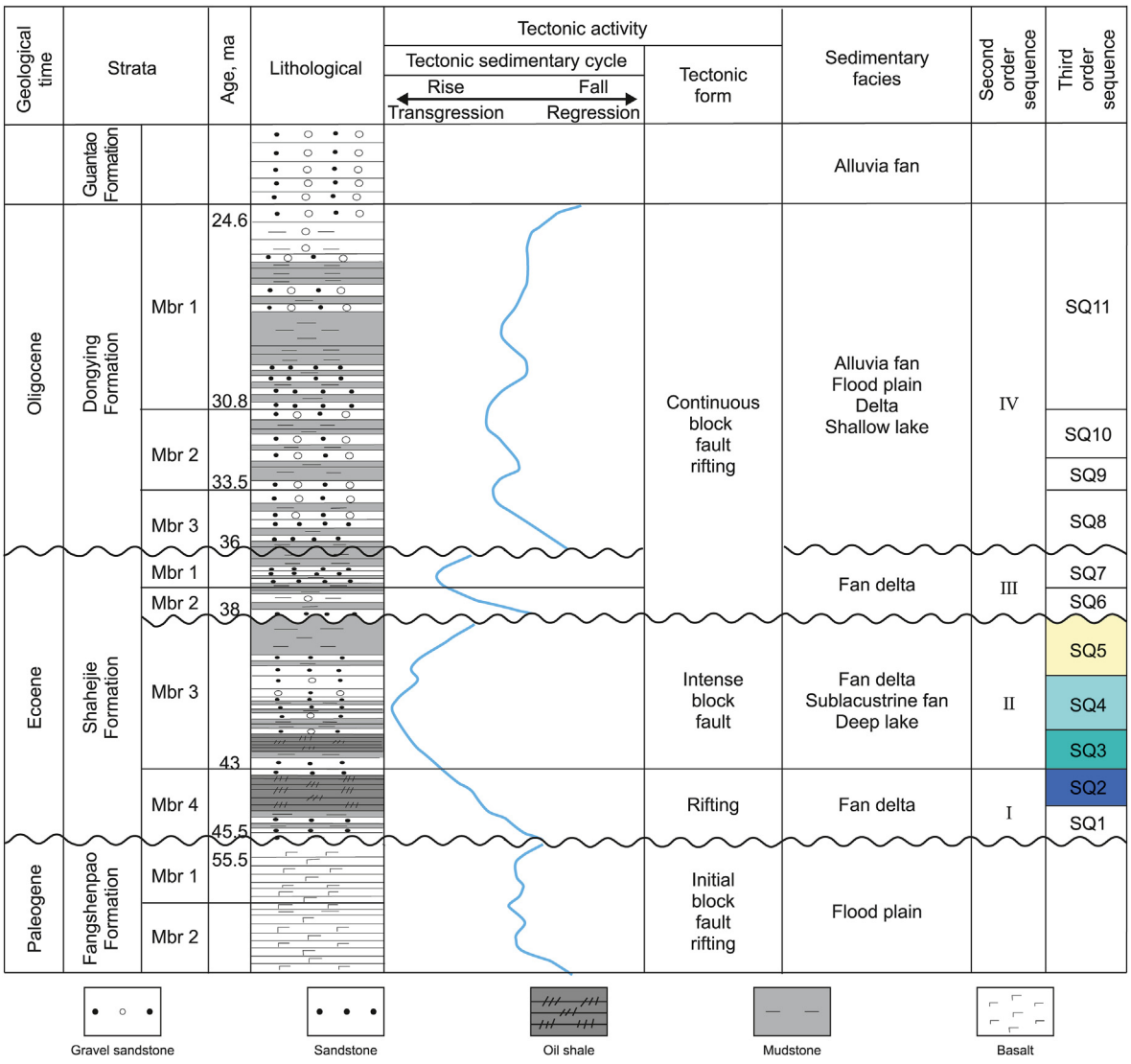

Fig. 2. The generalized stratigraphic column shows the lithology, carrier beds, tectonic history, and sedimentary facies of the Western Depression.

(Dai, 1992, 1993; Liu et al., 2019). These three types of natural gas have all been found in the Bohai Bay Basin (Liu et al., 2019; Pei et al., 2022). The complexity of tectonic movements, the sedimentary system, and the variety in organic matter input have resulted in a mixture of kerogen types (humic, sapropelic, and mixed), which coexist in the basin (Xu et al., 2022). It is difficult to accurately depict the geochemical features of the organic matter in lacustrine rift basins using the limited measured geochemical data. Several methods have been proposed in previous studies, for example, incorporating well logging data, seismic attributes, depositional system analysis, and sequence stratigraphic characteristics into conventional regular source rock assessment (Passey et al., 2010; Lai et al., 2020b; Sahoo et al., 2021; Zeng et al., 2021, 2022) However, the majority of past research has concentrated on the estimation of total organic carbon content, leaving the prediction of spatial distribution of mudstones and kerogen types relatively unexplored. This aspect is essential for assessing the effectiveness of gas source rocks and thus warrants further investigation.

Geological modeling leverages the foundational principles of geological statistical modeling, a discipline initially rooted in the mining industry that has since been applied to the oil and gas sector (Cannon, 2018). The integration of geological statistical methodologies with geological data and stochastic modeling techniques enables the creation of more precise three-dimensional geological models. These models provide a richer understanding of the intricacies and uncertainties of subsurface environments. Stochastic modeling approaches are commonly used to account for the spatial variability of reservoir properties, such as porosity (Ali et al., 2022). Renowned methods in this domain include Sequential Indicator Simulation (SISIM), Sequential Gaussian Simulation (SGSIM), Object-based Modeling (OBM), and Multiple-Point Statistics (MPS) (Alabert and Massonnat, 1990; Al-Mudhafar, 2017). These techniques each have their strengths and weaknesses, and the choice between them often depends on the nature of the data and the specific objectives of the study.

This study aims to propose an approach to identifying and predicting effective gas source rocks in lacustrine basins, taking the Western Depression of the Liaohe Subbasin as an illustration. The gas source rocks in the depression were classified in line with genetic types of natural gas. A practical three-dimensional (3D) model was constructed using 3D modeling and facies-control modeling technologies to accurately depict the spatial distribution of effective gas source rocks and predict the geochemical characteristics of the organic matter (Damsleth et al., 1992; Zhang et al., 2008; Yang

and Zou, 2019). Exact descriptions of effective gas source rocks can provide supporting evidence for gas-source correlation and natural gas resources estimation, facilitating future natural gas exploration.

2. Geological setting

The Liaohe Subbasin, part of the Bohai Bay Basin, is a wedge-shaped rift basin in northeastern China, which is conventionally divided into the Western, the Eastern, and the Damintun Depressions (Fig. 1a) (Hu et al., 2005). The study area is located in the southern part of the Western Depression. A 3D seismic survey has been carried out in the area, covering c.a. 1424.8 km^2 (Fig. 1b). The Western Depression can be further divided into three structural units (from northwest to southeast): the gentle slope zone, the central structure zone, and the steep slope zone (Fig. 1c). The Paleogene is comprised of three formations (from bottom to top): the Fangshenpao Formation (Fm), the Shahejie Fm, and the Dongying Fm. (Fig. 2). The evolution of the Liaohe Subbasin was initiated by three-phase rifting during the Eocene-Oligocene, which led to the separation of the Western Depression (Fig. 1b and 2) (Li, 1981; Qi and Yang, 2010). The first phase was part of initial rifting that formed west-dipping extensional faults. The Fourth member (Mbr 4) of the Shahejie Fm. slowly filled in the depression, forming fan delta and lacustrine deposits. Rapid subsidence occurred during the second stage of deep rifting, resulting in southwest-northeast faults. Mbr 3 of the Shahejie Fm reached maximum depositional area and thickness during this stage, with deposition dominated by fan delta-deep lacustrine-turbidite systems. The third stage coincided with the depositional period of the first and second members of Mbr 1 and Mbr 2 of the Shahejie Fm and the Dongying Fm, showing continuous rifting attenuation, which formed minor east-west faults. The lake was shrinking during this period, and fan delta and shallow lake deposits prograded. (Fig. 2) (Wang et al., 1985; Li, 2020).

This study focuses on Mbr 3 and Mbr 4 of the Shahejie Fm, which are the primary gas-generating and gas-producing layers (Li et al., 2013; Wang et al., 2019; Yang et al., 2019). Kerogen in the Mbr 4 of the Shahejie Fm source rocks varies between type I and type II.

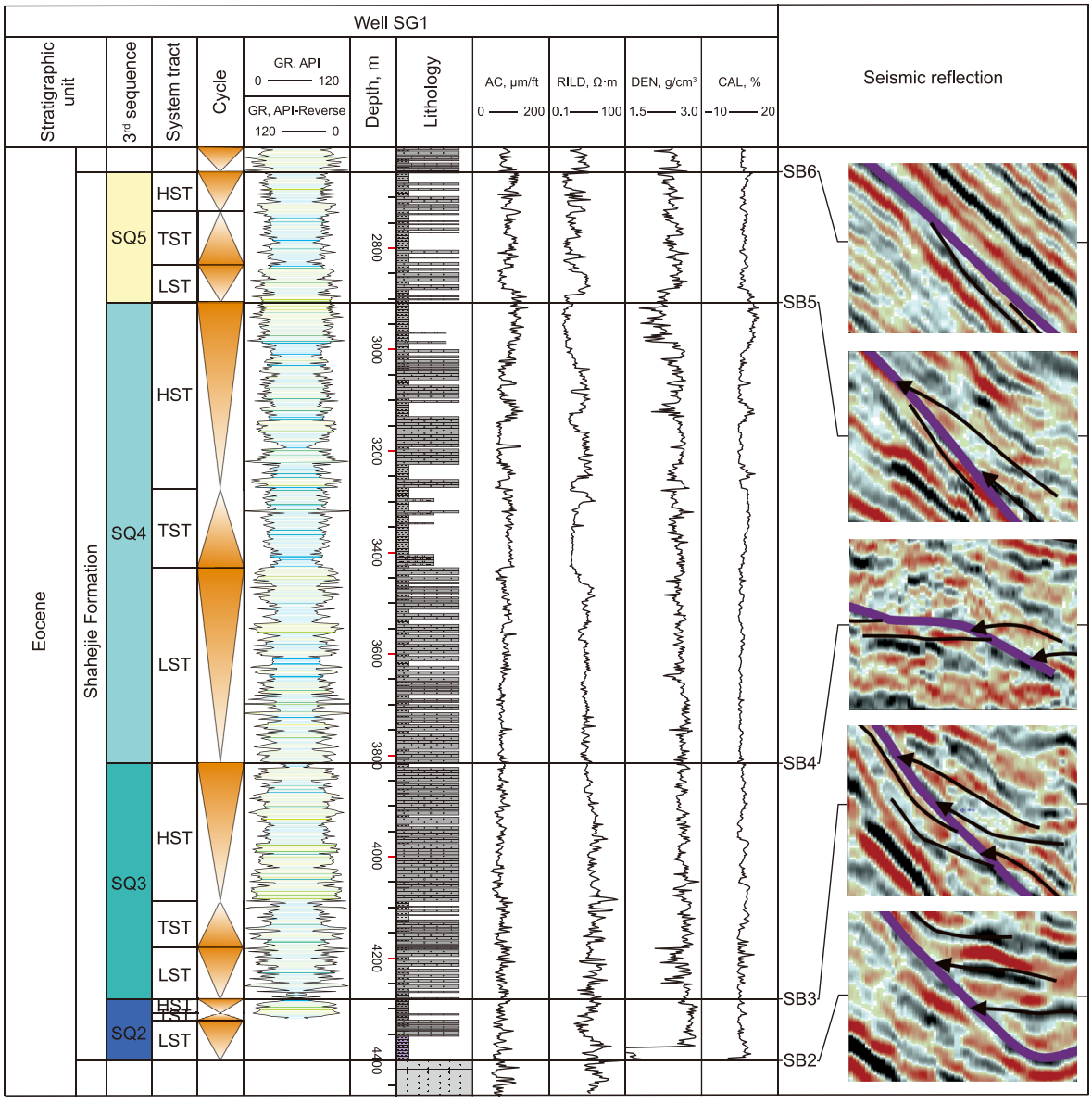

Fig. 3. Sequence stratigraphic division of well SG1 in the western Depression and representative seismic reflection characteristics of the major unconformities in examples.

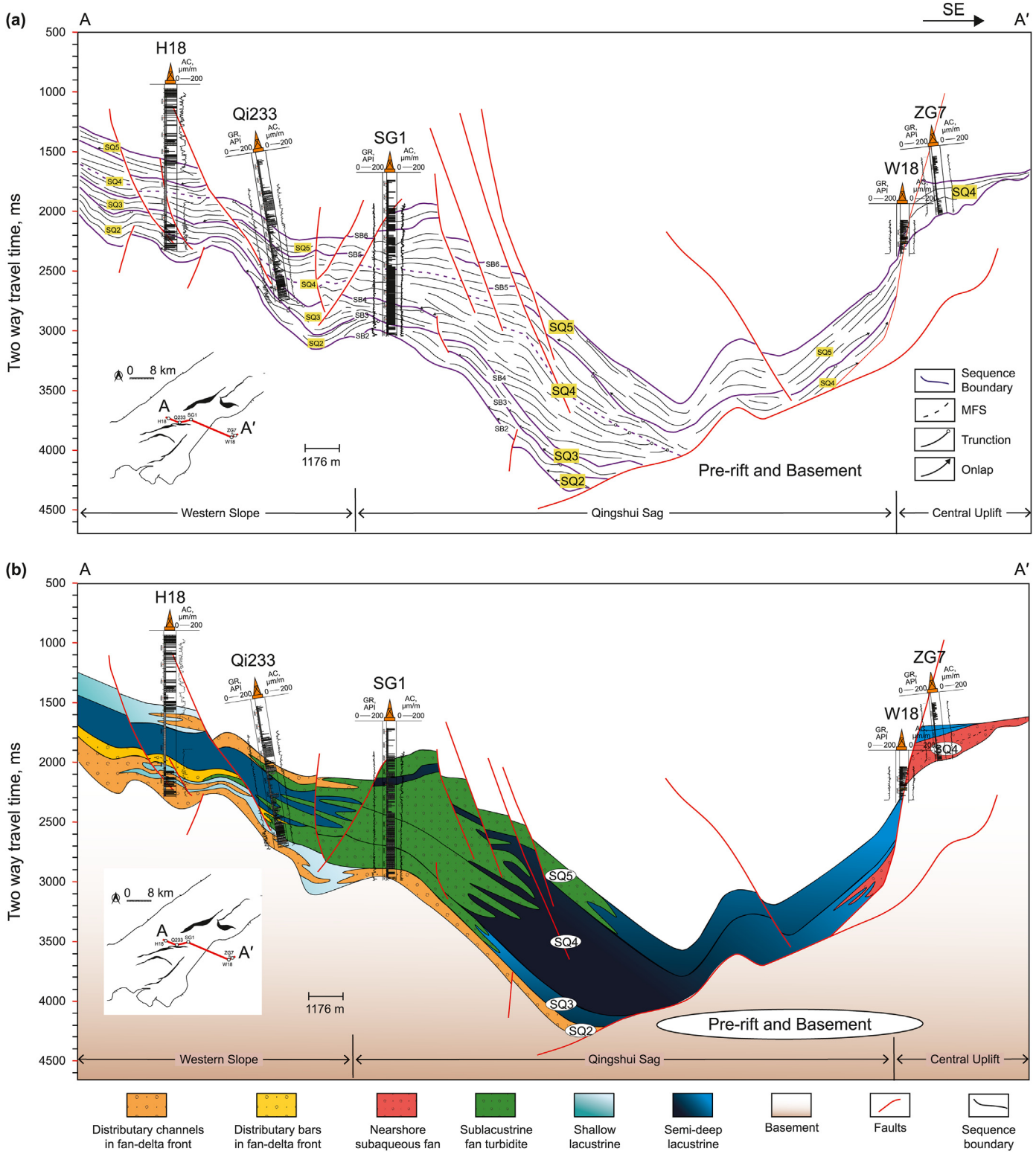

Fig. 4. Interpretative line drawing of a seismic section in the central part (crossing wells H18 and ZG7) of the Western Depression. (a) interpretative line drawings illustrating the basin architecture and the seismic reflection character of sequence boundaries and basin fills. (b) schematic diagram showing the depositional system types and trends; SB: sequence boundaries; SQ: third-order sequence; Location of the seismic section is marked in Fig. 1, Line AA'.

The Mbr 3 of the Shahejie Fm contains mainly type II or mixed type II/III kerogens (Hu et al., 2005). Mbrs 3 and 4 of the Shahejie Fm can be divided into four three-order sequences, SQ5, SQ4, SQ3, and SQ2, which correspond to the upper Mbr 3, middle Mbr 3, lower Mbr 3, and upper Mbr 4 of the Shahejie Fm, respectively (Mu et al., 2010). The SQ1, corresponding to the lower Mbr 4 of the Shahejie Fm, is absent in the study area and mainly occurred in the northern part of the Western Depression (Xie et al., 2010). The gas reservoirs in the

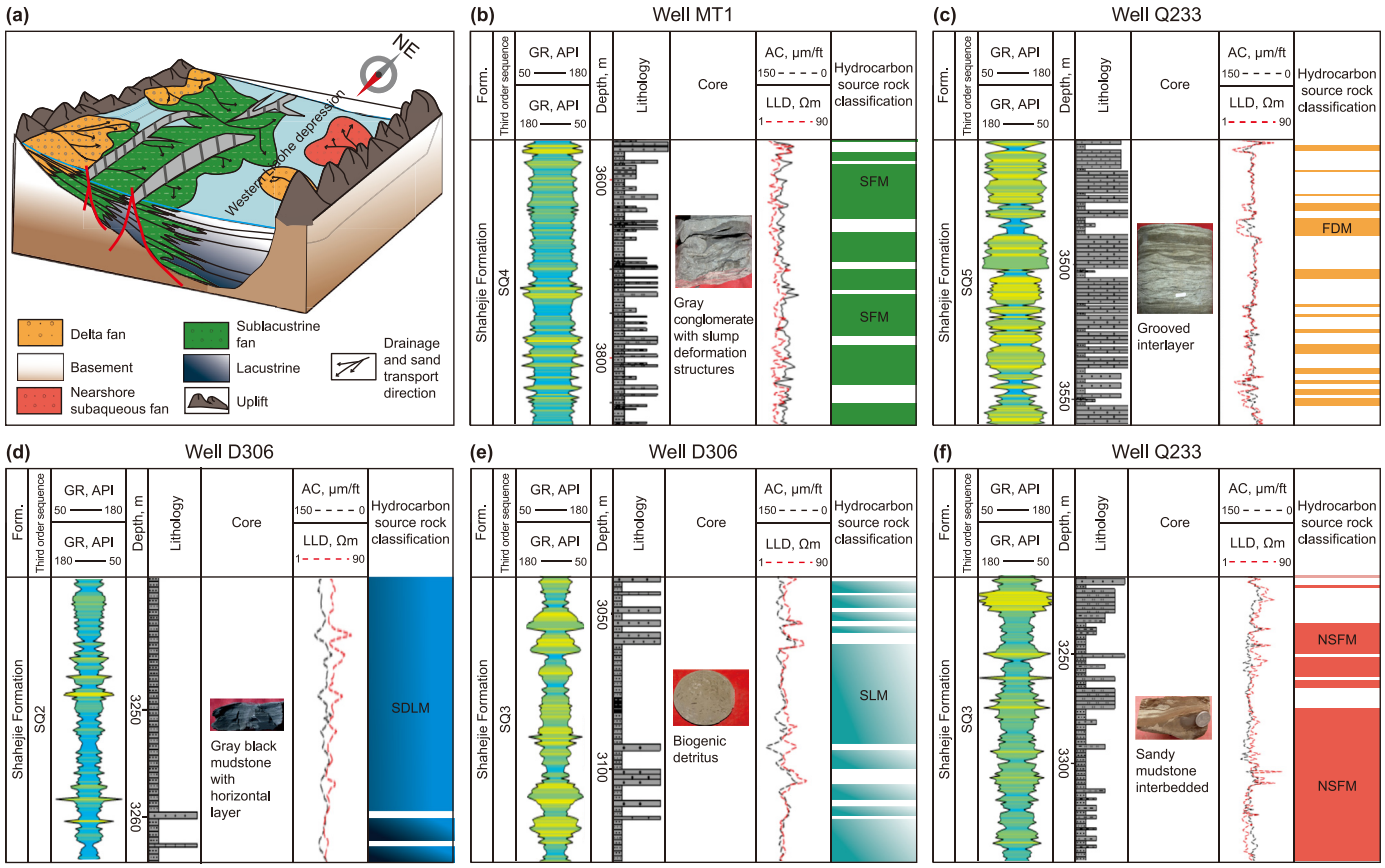

Fig. 5. (a) Depositional model of the Shahejie Formation in the Western Depression. (b)–(e) The lithological, core and logging characteristics of various source rock types in the representative wells; GR: gamma-ray logging; LLD: deep lateral resistivity logging; AC: acoustic logging.

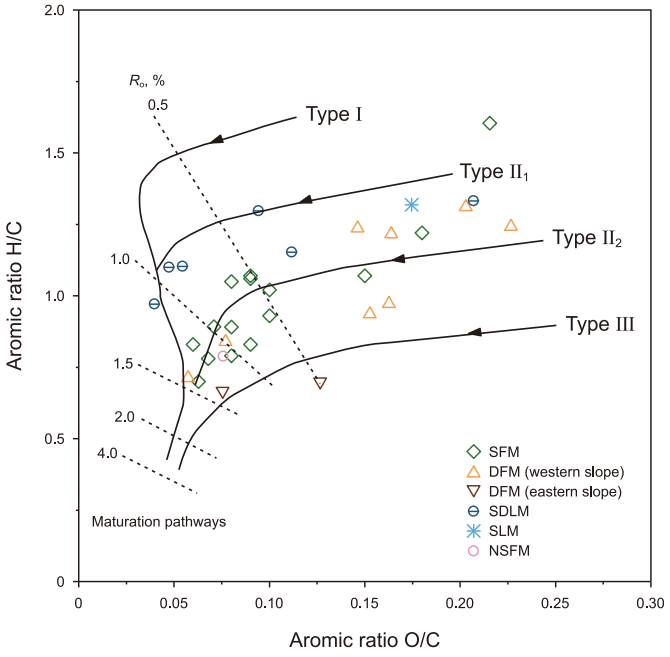

Fig. 6. Plot of kerogen atomic H/C versus O/C showing the kerogen types of mudstone samples from different sequences of the Shahejie Formation (modified after Peters, 1986).

Shahejie Fm are the most explored (Huang et al., 2017). The Huangxiling gas reservoir, which contains predominantly oil-type gas (Wang et al., 2018), is in the southern gentle slope zone, adjacent to the Qingshui and Yuanyanggou Sags (Fig. 1). The Xinglongtai buried hill is a structural belt extending northeast and surrounded by the Qingshui and the Panshan Sags (Fig. 1). Microbial gas reservoirs are found in shallow strata (<2000 m depth) overlying the buried hill. The natural gas inside the buried hill is dominated by thermogenic gas originating from the Mbr 3 of the Shahejie Fm source rocks in the Qingshui Sag (Pei et al., 2022).

3. Materials and methods

3.1. Materials

Thirty-four mudstone samples from four target sequences (SQ2-SQ5) in well MT1 were selected for geochemical analysis. For the analysis of the total organic carbon (*TOC*) content and the Rock-eval pyrolysis, all the samples were prepared. Experimental geochemical data provided by the CNPC Liaohe Oilfield Exploration and Development Research Institute were used for hydrocarbon source rock evaluation. These data were from 1004 mudstone samples spread throughout the study area and included *TOC* contents, hydrocarbon generation potential (S_1+S_2), vitrinite reflectance (R_o), maximum pyrolytic temperature (T_{max}), and element contents (C, H, and O). The location of the sampled wells is shown in Fig. 1b. Forty-seven well-logging curves, a 3D seismic survey, and three

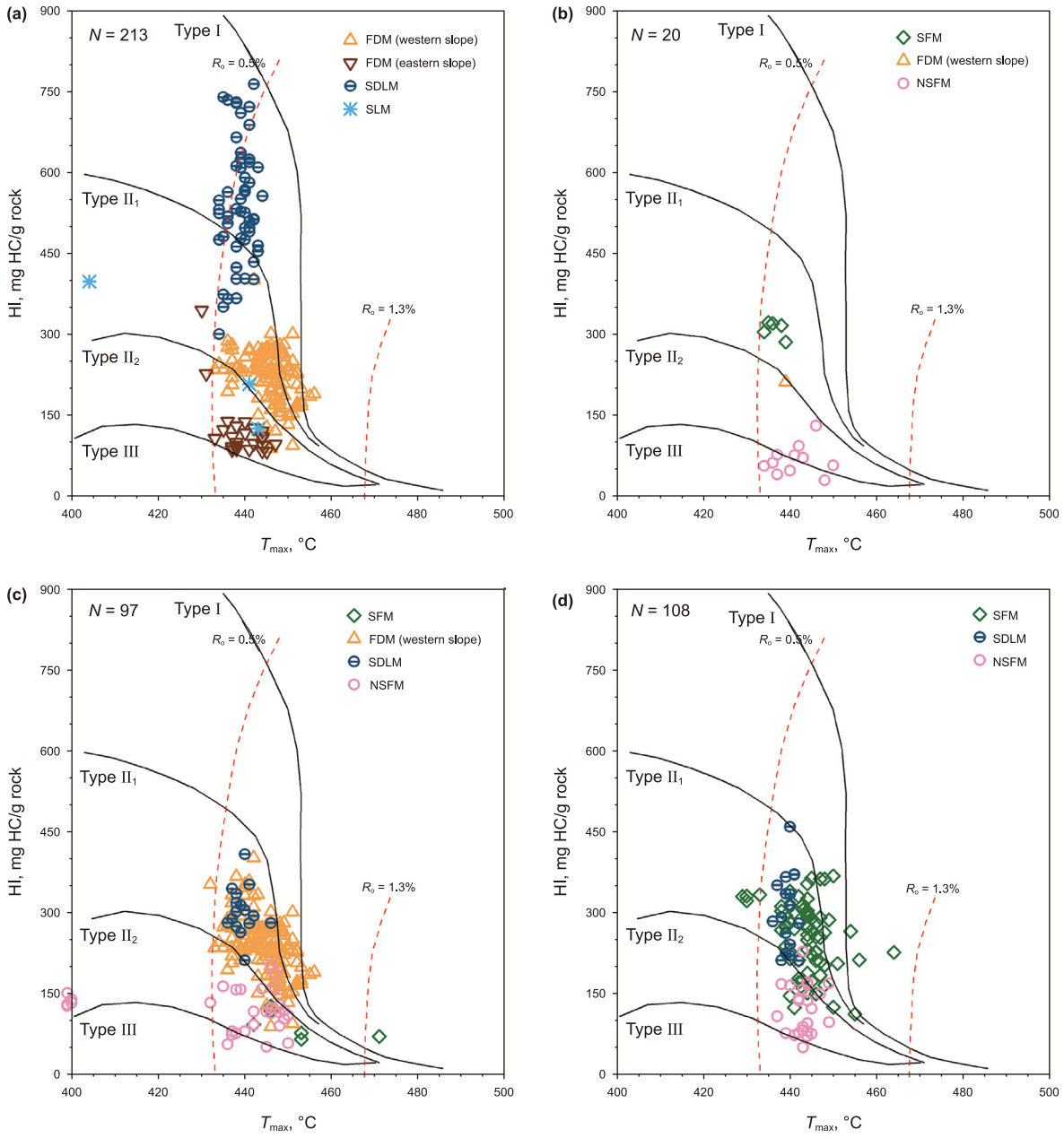

Fig. 7. Plots of HI versus T_{max} showing the kerogen types of mudstones from different sequences of the Western Depression; (a) SQ2, (b) SQ3, (c) SQ4, (d) SQ5 (modified after Bordenave et al., 1993).

vertical seismic profiles (VSPs) were also collected to build 3D geological models.

3.2. Methods

3.2.1. Laboratory experiments

TOC analysis was carried out on mudstone samples crushed to 80 mesh powder. Dilute hydrochloric acid (1.5 mol/L) was used to remove carbonates from the samples. The samples were then cleaned with deionized water to remove any residual contamination. A LECO CS-230 carbon analyzer was used to measure the *TOC* contents of the processed samples (Table S1).

For the rock-eval pyrolysis experiment, mudstone samples were crushed to 100 mesh and heated in a Rock-Eval II instrument. The volatile hydrocarbon S_1 (mg HC/g Rock) reached its maximum area at a temperature of 300 °C. The peak area for pyrolytic hydrocarbon S_2 (mg HC/g Rock) was obtained at 300 °C–500 °C. The maximum temperature reached during the acquisition of S_2 is the peak temperature of pyrolysis (T_{max}) (Peters and Cassa, 1994; Behar et al., 2001). (Table S1)

3.2.2. TOC estimation model

The 3D surface fitting technique proposed by (Zeng et al., 2021) was employed to predict organic-rich mudstone interbeds in the study area, using measured *TOC* data overlaid by resistivity, porosity logs, and gamma logging curves. *TOC* estimation was carried out in MATLAB 2016a.

3.2.3. Three-dimensional geological modeling

The 3D source rock model developed in this study derives the

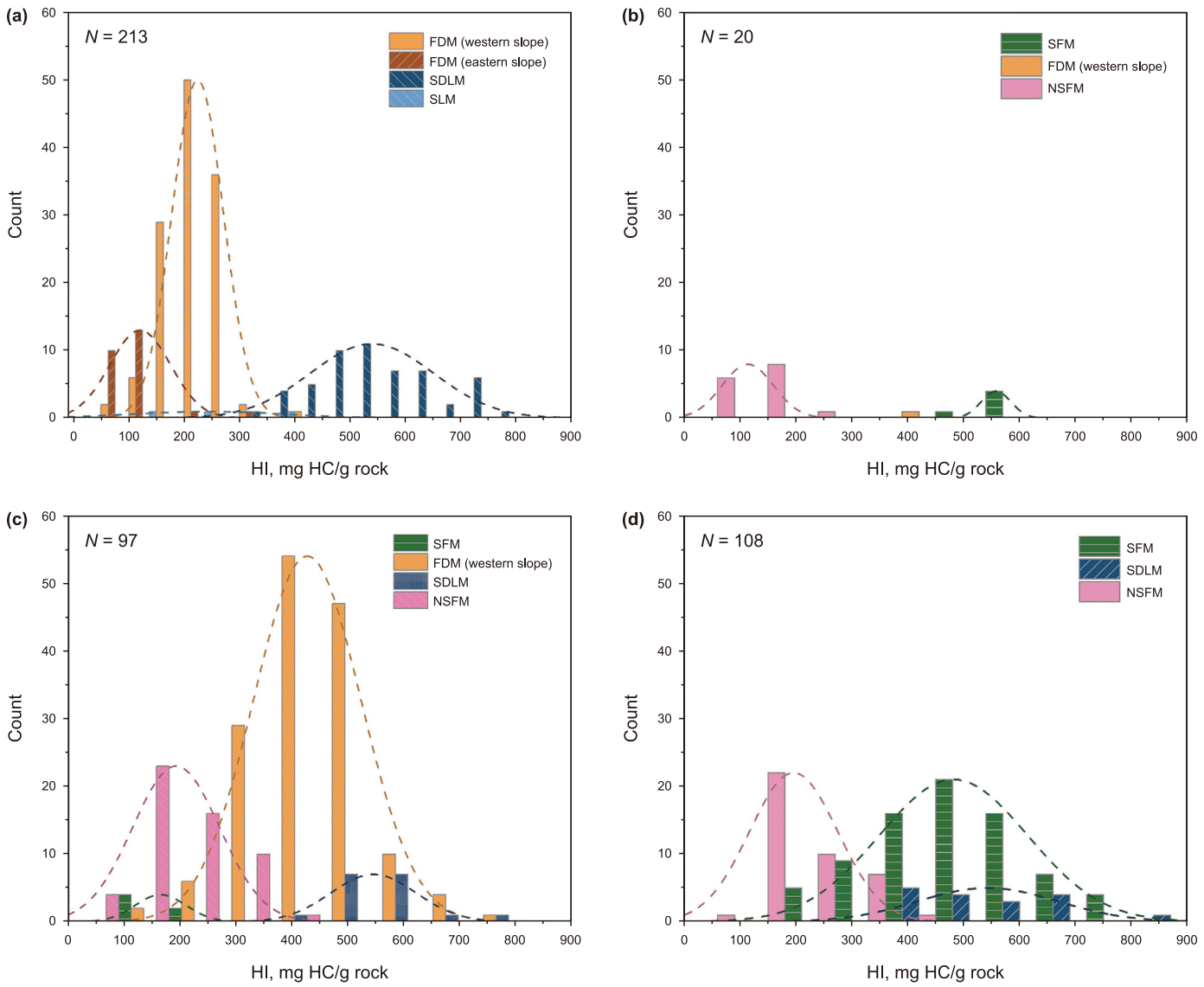

Fig. 8. Histogram showing the Gaussian distribution of HI for each type of mudstone in the Western Depression within the sequence stratigraphic framework; (a) SQ2, (b) SQ3, (c) SQ4, (d) SQ5.

three-dimensional distribution characteristics of source rocks from structural, lithofacies, and petrophysical distribution models (Zhang et al., 2008; Yang and Zou, 2019; Ali et al., 2022; Anees et al., 2022). The modeling was conducted in Petrel™ Schlumberger Modelling software.

The available data were imported into the software to build a 3D structural model: Two-way time (TWT) surfaces were constructed by interpreting the seismic data, including seismic-to-well ties, faults, and sequence boundaries. An advanced velocity model converted these surfaces to depth structure surfaces. The structure model was constructed by fault modeling, pillar gridding, and formation extraction and contained information on the relative positioning between stratigraphy and faults. This will provide an effective framework for further modeling (Khattab et al., 2023).

The characteristics of the sandstone and mudstone lithofacies were updated with the analysis of logging data. Mudstone types were classified based on their sedimentary systems and regional depositional context. A sedimentary facies model was established by geometric modeling following the division of sedimentary facies set out in previous studies (Gao et al., 2017; Wang et al., 2019; Li, 2020). The lithofacies model used the sequential indicator simulation method (SISM), constrained by the sedimentary facies model as a specified probability trend.

Three-dimensional property modeling consisted of three geochemical parameter models: *TOC*, HI, and R_o. The distribution of geochemical properties, including HI and *TOC*, was modeled using spatial variograms to populate the model. For each type of mudstone, separate *TOC* and HI modeling was conducted. This was achieved by employing Gaussian random function simulations and incorporating facies-control and Co-kriging methods to account for trends. The R_o model was obtained by calculating the depth of the structure model using the fitting formula of R_o-depth in the study area.

4. Results

4.1. Sequence-stratigraphy framework and sedimentology

The detailed sequence stratigraphic-geochemical analysis in this study was carried out by detailing the sequence-stratigraphic

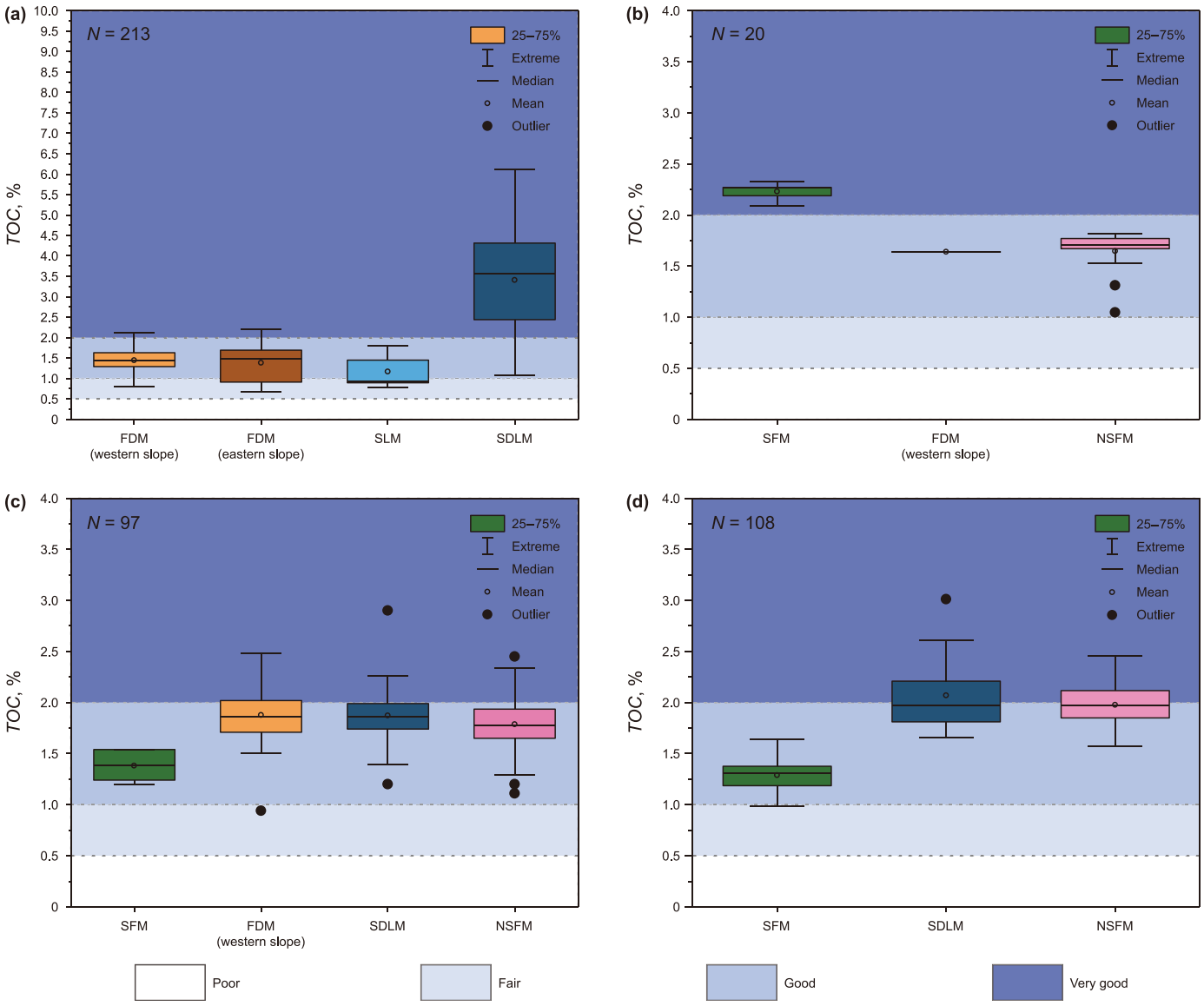

Fig. 9. Organic matter abundance in the Shahejie Formation, Western Depression, Liaohe Subbasin; (a) SQ2, (b) SQ3, (c) SQ4, (d) SQ5 (From Peters, 1986).

framework and depositional properties of the source beds. (Lai et al., 2020a,b). Previous investigations have covered the sequence-stratigraphic framework, depositional systems, and the Shahejie Fm in the Western Depression. (Wang et al., 2010; Xie et al., 2010; Feng et al., 2016; Gao et al., 2017). Six angular unconformities (SB2, SB3, SB4, SB5, and SB6, from bottom to top) form sequence boundaries that divide the Mbrs 3 and 4 of Fm into four third-order sequences (SQ2, SQ3, SQ4, and SQ5) (Feng et al., 2016; Mu et al., 2010; Wang et al., 2010; Xie et al., 2010). A stratigraphy framework was established by tracing onlap or truncation surfaces on a 3D seismic survey and identifying sudden lithology and grain size changes in well-log data (Figs. 3–4a). A thorough analysis of depositional cycles corresponding to parasequence sets confirmed the third-order sequence division scheme of the Middle Eocene succession (Fig. 3).

The slope belt of the Western Depression, which has experienced rapid deposition rates, storage, movement, and transformation of organic materials in addition to the deposition of terrigenous clastic material, is a synergism zone of several sedimentary facies (Anas et al., 2015; Zhu et al., 2022). Four types of depositional systems were developed in the Western Depression: fan delta, alluvial fan, lacustrine deposits, and sublacustrine fan (Hu et al., 2005; Gao et al., 2017; Li, 2020). These depositional systems were identified based on an analysis of their lithologies, and the depositional environment revealed the stratigraphic sequence framework (Figs. 4–5a).

During the SQ2, fan delta sediments were deposited in a shallow water environment from the initial rifting stage. The lake began to expand during SQ3, and sublacustrine fans were deposited in front of the fan delta deposits from the SQ2 period. The basin experienced its most extensive transgression during the SQ4 when sublacustrine fans and semi-deep lacustrine were widely deposited (Fig. 4).

4.2. Classification of mudstone types

The accumulation of organic matter (OM) is fundamentally governed by the sedimentary environment, along with the preservation and productivity conditions it offers. In the study area, we distinguished five distinct types of mudstones, classified according

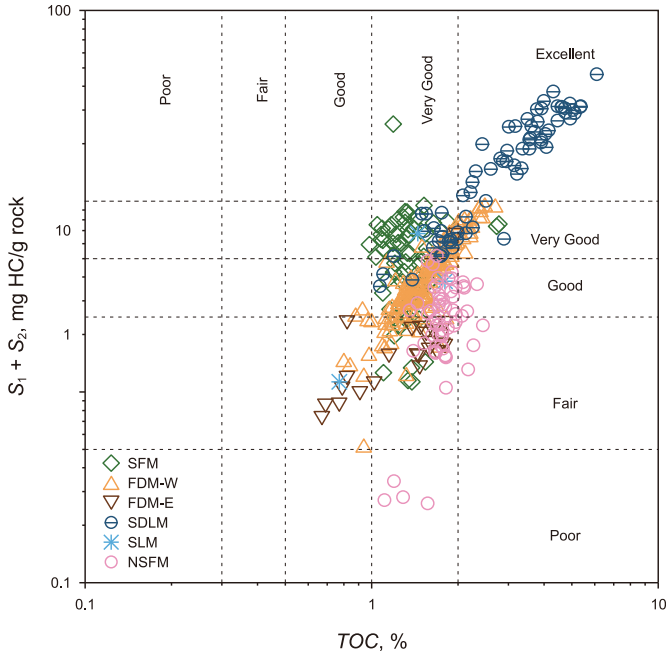

Fig. 10. Plot of *TOC* versus S_1+S_2 showing the organic richness and hydrocarbon generative potential of different types of source rocks within the Shahejie formations.

to the sedimentary characteristics of the Shahejie Fm.

(1) Sublacustrine fan mudstones (SFM) were derived from muddy deposits between turbidite channels and a thin layer of lacustrine deep-water mudstones between the two sets of turbidites. The alternating layers of thin sands and mudstones generated a succession of kicks or spikes on the gamma-ray log (GR) curves (Fig. 5b).

(2) Fan delta mudstones (FDM) developed locally on the western gentle slope (FDM-W) and the eastern steep slope (FDM-E). The lithology is repeatedly stacked with sandstone and sand conglomerate longitudinally, with medium-low amplitude dentate bell or box-shaped bell GR curves (Fig. 5c).

(3) Semi-deep lake mudstones (SDLM) were deposited in the center sags in a deep lacustrine water environment. The lithofacies are composed of sandy mudstones with thin-graded sandstone strata and black mudstones that lack structure or are laminated. Their GR curves are linear forms with low amplitude (Fig. 5d).

(4) Shallow lake mudstones (SLM), including fine-grained sediments, accumulated between the former delta and the shallow lake. Gray mudstones, thinly laminated siltstones interbedded, and fine-grained sandstones comprise the lithofacies (Fig. 5e).

(5) Nearshore subaqueous fan mudstones (NSFM) formed locally on the northeast side of the Western Depression. The deep-

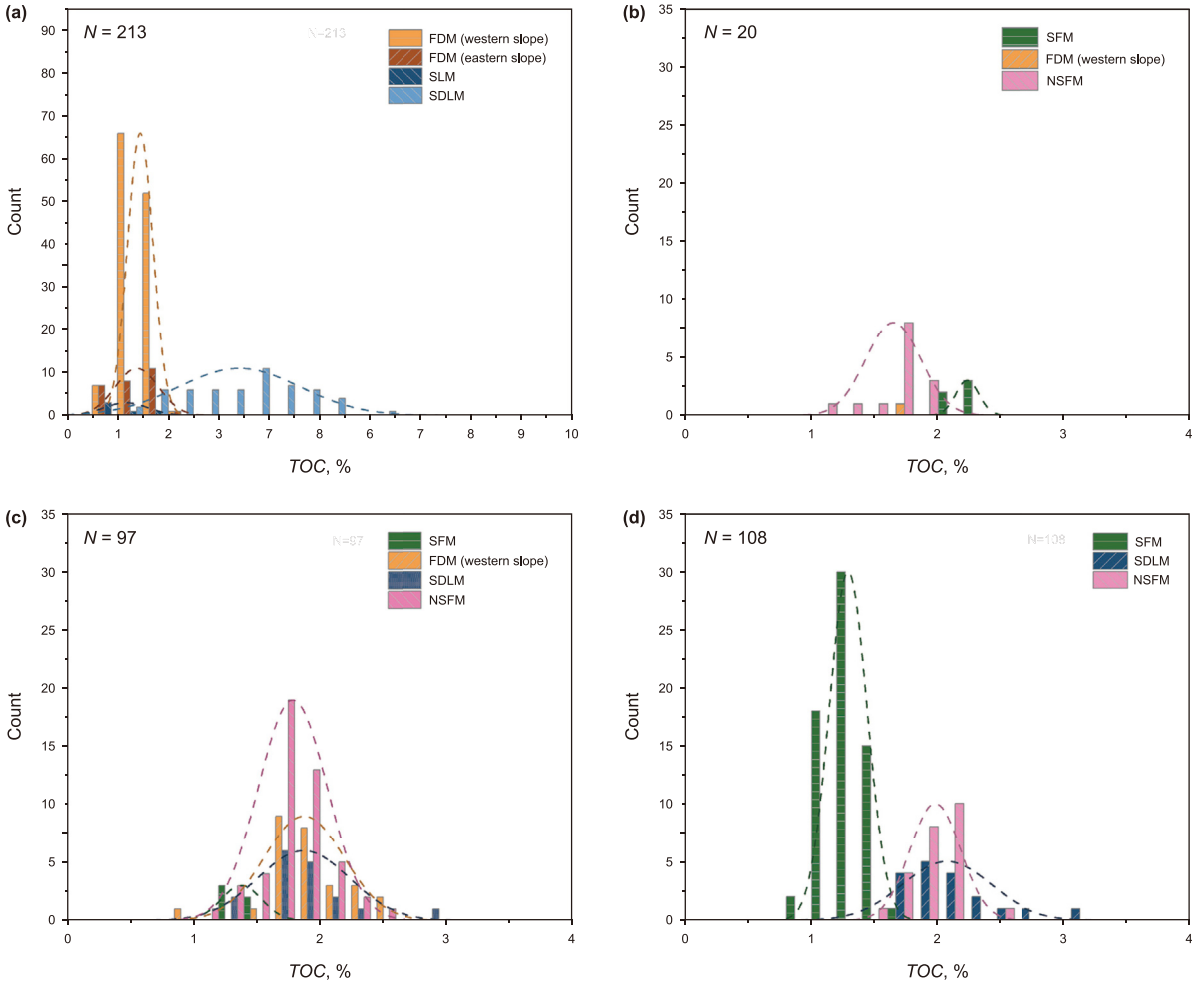

Fig. 11. Histogram showing the Gaussian distribution of *TOC* contents for each type of mudstone in the Western Depression within the sequence of layers; (a) SQ2, (b) SQ3, (c) SQ4, (d) SQ5.

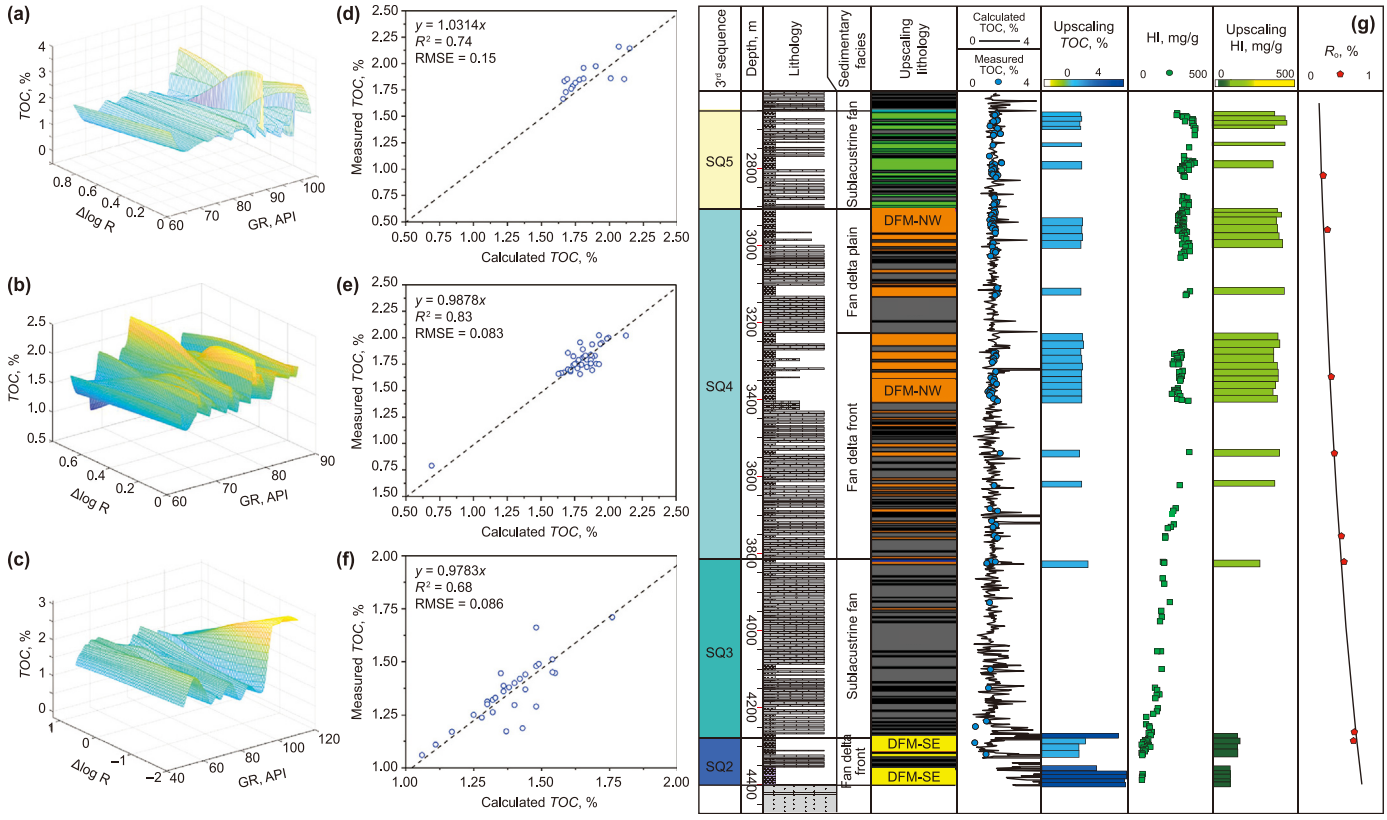

Fig. 12. (a)–(c) The biharmonic interpolation surface created using *TOC*, GR, and ΔlogR data from Wells MS1/MT1, SG1, and S202, respectively. (d)–(f) Comparison of predicted *TOC* and measured *TOC* of each model; (g) Predicted *TOC* content results and geochemical profile of Well SG1.

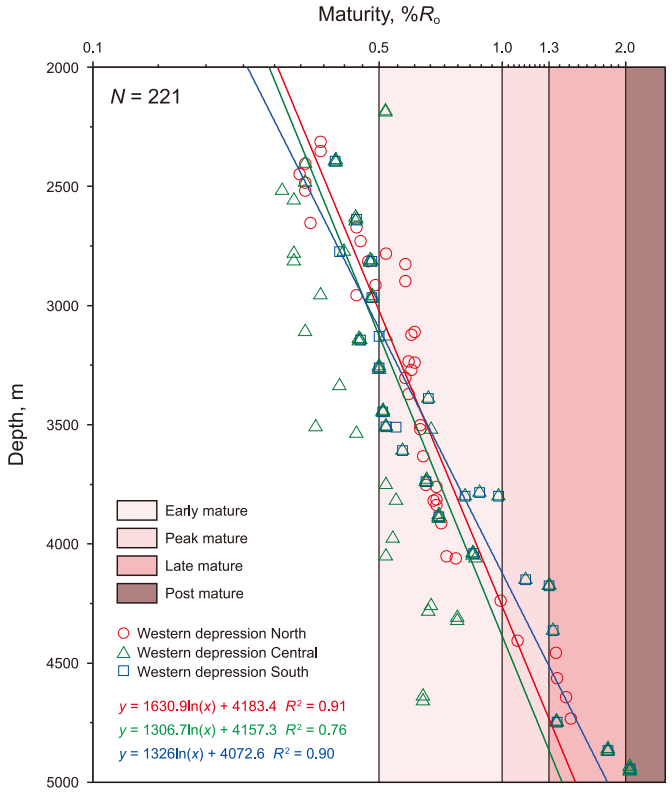

Fig. 13. Fitting study between R_o data and the corresponding depths in the Western Depression, with well S202 representing the northern side, wells SS3 and SG1 representing the central section, and well MS1 representing the southern side of the study area.

lacustrine mudstone intervals are thick, dark gray, and interbedded with coarse-grained fan deposits. A sequence of kicks or spikes, like SFMs, were created on the GR curves as a result of the alternating of thin sands and mudstones. (Fig. 5f).

4.3. Geochemical properties

4.3.1. Organic matter types

The nature and intensity of organic matter hydrocarbon

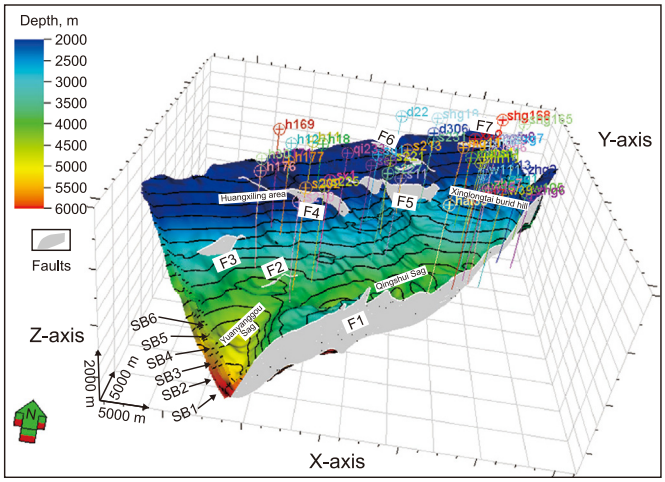

Fig. 14. 3D structural model of the Shahejie Formation in the Western Depression. (a) SQ2, (b) SQ3, (c) SQ4, (d) SQ5, SB: Sequence boundary.

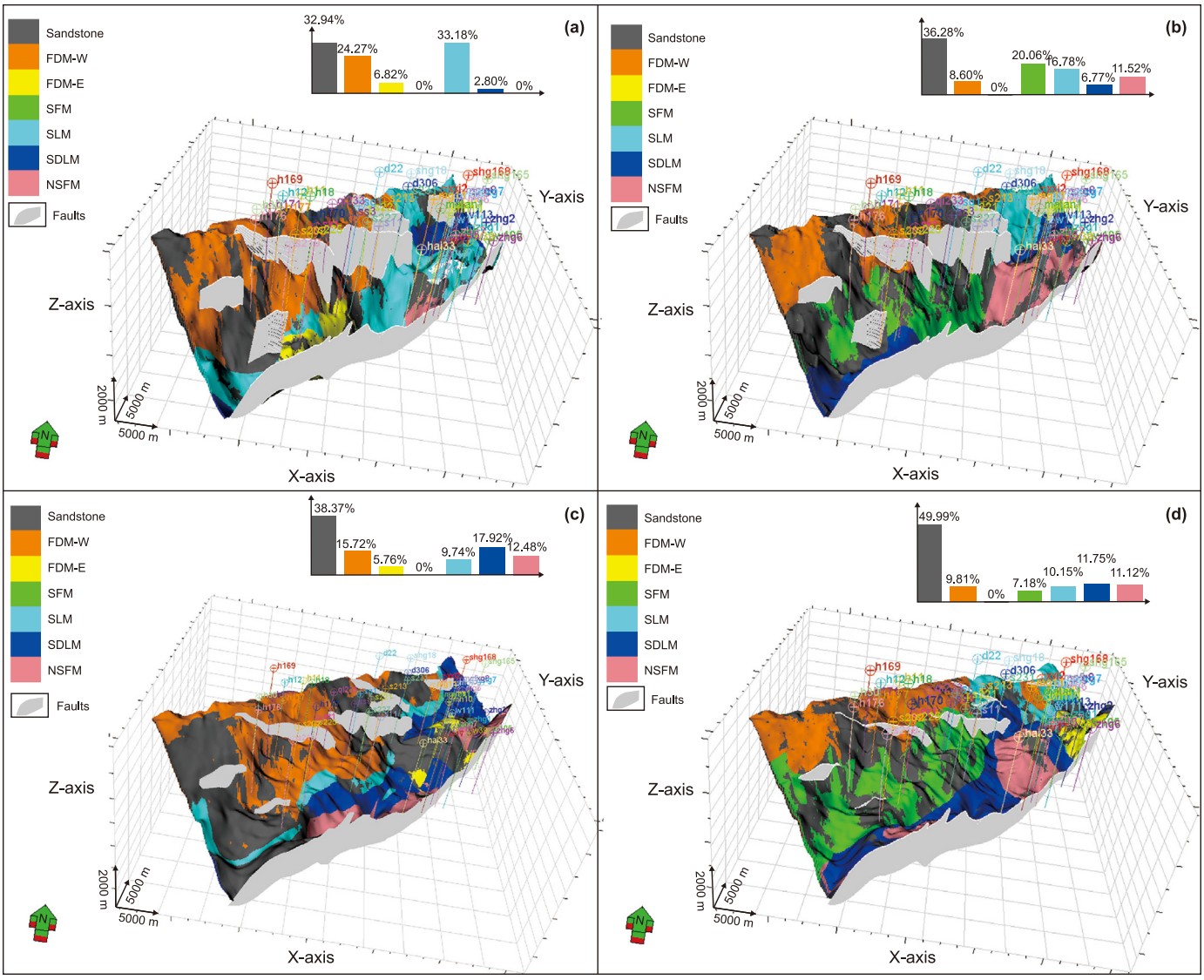

Fig. 15. 3D facies models of the Shahejie Formation in the Western Depression; (a) SQ2, (b) SQ3, (c) SQ4, (d) SQ5. SFM: Sublacustrine fan mudstones; FDM-W: Fan delta mudstones, developed locally on the northwestern gentle slope; FDM-E: Fan delta mudstones developed locally on the northeastern steep slope; SDLM: Semi-deep lake mudstones; SLM: Shallow lake mudstones; NSFM: Nearshore subaqueous fan mudstones.

generation are directly related to the quality of the kerogen. H/C versus O/C and HI versus T_{max} have been commonly used plots for classifying organic matter types (Hunt, 1981; Bordenave et al., 1993). Figs. 6 and 7 show that SDLMs, SFMs/SLMs, and NSFMs are dominated by types II_1, II_2, and III, respectively. FDMs occur in the western gentle and eastern steep slopes, which have predominantly type II_2 and III, respectively (Figs. 6 and 7a-c). The distribution of organic matter types shows a remarkable correlation with the tectonic position in which the sedimentary facies are located. The mudstones on the western gentle slope contain mainly type II_2 organic matter, the center of the depression contains mainly type II_1 organic matter, and the steep slope zone contains mainly type III organic matter. The histogram of the geochemical data must be in Gaussian form (normal distribution) so that geostatistical methods can be applied to predict the distribution of geochemical parameters (Azevedo and Soares, 2017). Unlike mudstone samples from each sequence, the HI of each type of mudstone shows a Gaussian distribution (Fig. 8). The deterministic components of organic matter types—sedimentary systems—have been eliminated.

4.3.2. Organic matter abundance

TOC—the total amount of organic matter present in the sediment—is an indicator of the hydrocarbon-generating potential of the sediment (Dembicki, 2009). A box-plot is a statistical graph describing the discrete degree of a data group and reflects the stability of optimization effects. Fig. 9 shows that almost all samples in the Western Depression represent good source rocks (*TOC* contents greater than 1.0%). SDLMs in SQ2 and SFMs in SQ3, in particular, are very good source rocks, with median *TOC* content of 3.3% and 2.2%, respectively (Fig. 9a and b). The *TOC* content of SDLMs in SQ4 and SQ5 generated large outliers of 2.9 % and 3.1%, respectively, which indicates that the *TOC* contents of SDLMs easily fall into the local extremum (Fig. 9c and d). The SLMs in SQ2 have the lowest median *TOC* contents, at 0.9% (Fig. 9a). When examining the relationship between S_1+S_2 (mg HC/g rock) and *TOC*, the data points representing SDLMs are situated in the region that denotes very good to excellent source rocks. In contrast, the data points pertaining to other mudstone types fall within the good to excellent source rock domain (Fig. 10). As shown in Fig. 10, compared to other

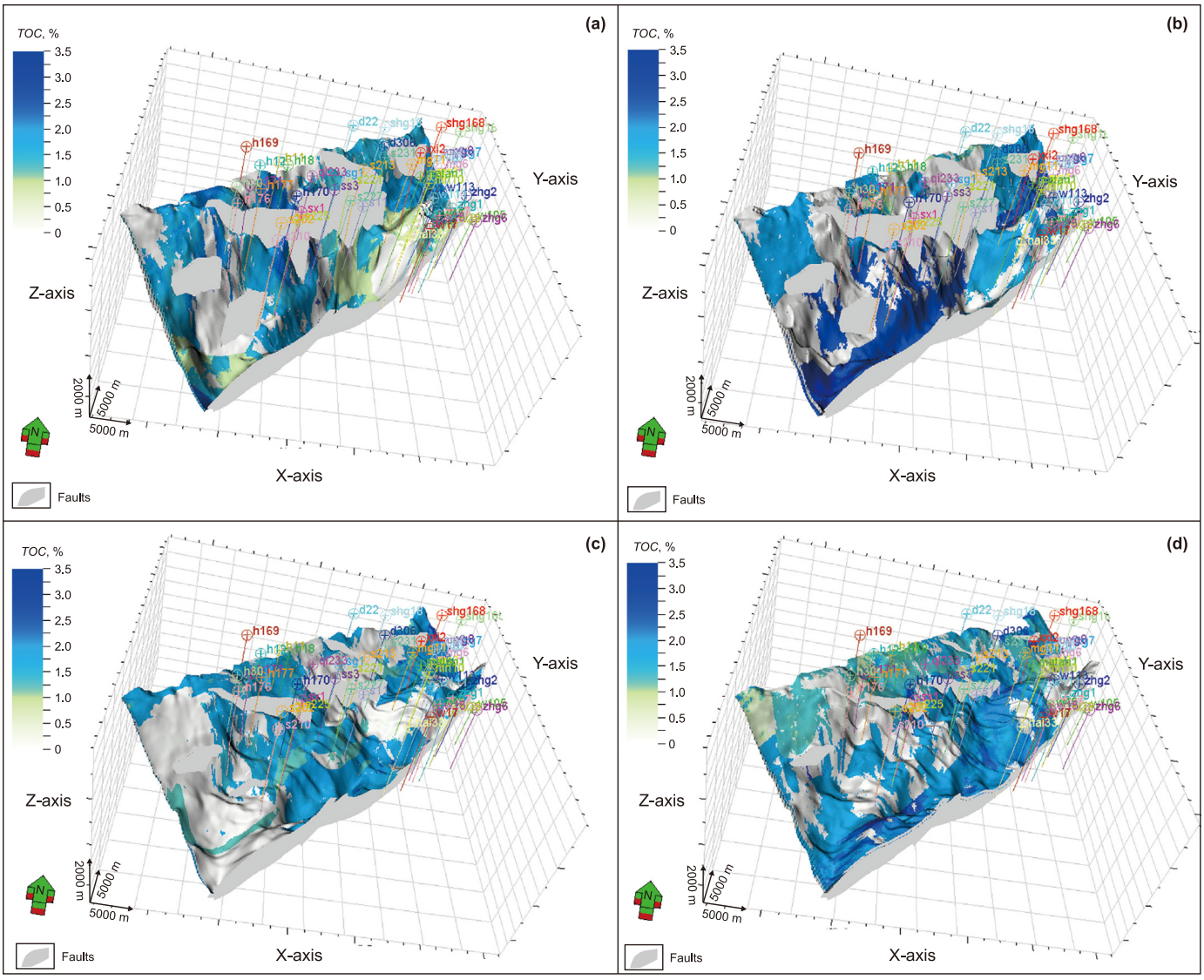

Fig. 16. The 3D *TOC* model of the Shahejie Formation in Western Depression.

source rocks, SDLMs consistently display a relatively higher concentration of organic matter. The *TOC* content distribution of each type of mudstone conforms to the normal distribution, which confirms the feasibility of facies-controlled modeling for *TOC* contents (Fig. 11).

The 3D surface fitting technique proposed by (Zeng et al., 2021) was applied to calculate *TOC* contents in this study, as it is particularly suitable for frequent sand mud interbedding. This method excels in reducing inaccuracies induced by continuous lithological shifts, thereby facilitating precise *TOC* estimations for mudstone interlayers. Crucially, the 3D surface fitting technique effectively differentiates between source and non-source rocks, which bears substantial significance for source rock evaluation and the selection of optimal source-reservoir-cap assemblages (Zeng et al., 2021). Fig. 12a–c displays the prediction models for the northern, central, and southern sections of the study area. These models are established based on three biharmonic interpolation surfaces formulated using data from wells MT1/MS, SG1, and S202, respectively. From Fig. 12d–f, it is apparent that the 3D surface fitting technique yields predictive results for both pure mudstone samples and interlayer mudstone samples. *TOC* curves were extrapolated for 35 wells within this region to provide sufficient data for the following 3D source bed modeling. This comprehensive analysis helps clarify the patterns of organic matter distribution in the study area.

4.3.3. Organic matter maturity

Vitrinite reflectance (R_o) is also widely accepted as a reliable reference, partly due to its widespread use. As shown in Fig. 13, R_o data varies differently with burial depth between mudstone samples from the southern, central, and northern parts of the Western Depression as a consequence of the different heat flow histories of the different tectonic locations (Hu et al., 2005). Three separate R_o-depth equations were constructed in building a thermal maturity model for this study. The current burial depths for the onset of oil generation on the southern side, in the central section, and on the northern side are estimated as 3053 m, 3252 m, and 3153 m, respectively. The bottoms of the oil windows occur at 4611 m, 4500 m, and 4420 m, respectively (Fig. 13).

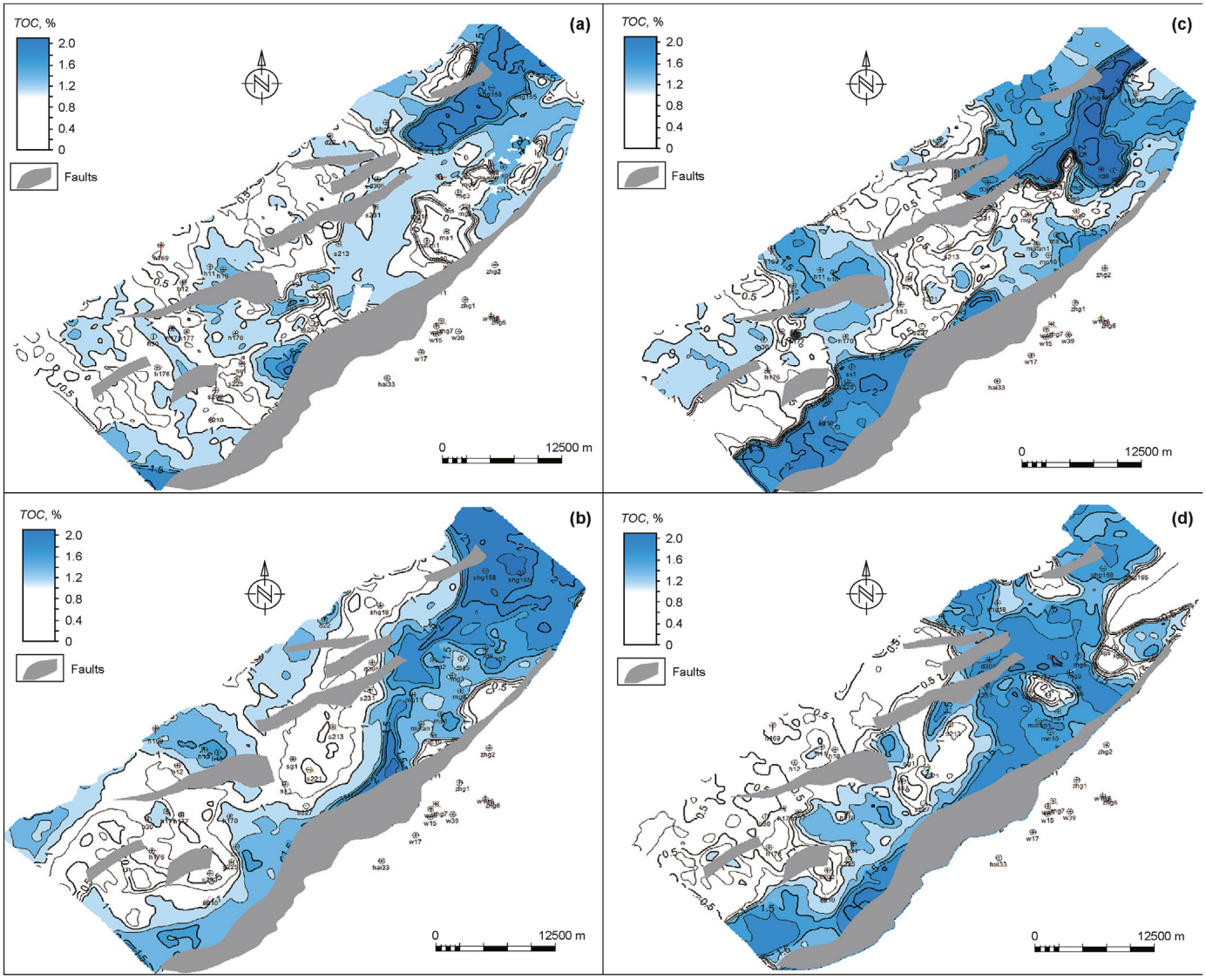

Fig. 17. Isogram showing the average *TOC* content of mudstones in different sequences of the Shahejie Formation in the Western Depression.

4.4. Three-dimensional geological model

4.4.1. Structural model

A structure model is a foundation and skeleton for predicting lithofacies and properties parameters. The Western Depression developed a two-stage fault system during the initial and deep rifting phase (Li, 2020). So, two fault zones were defined in the geological model: westward-dipping normal faults, including faults F1 (boundary fault), F2 and F3; and eastward-dipping normal faults, including F4, F5, F6, F7, and F8 (Fig. 14). Fault planes were generated in the 3D grid model (a framework in which the size of each grid was 100 m × 100 m × 20 m) by synthesizing and editing "Key Pillars." A 3D structure model was established by loading the stratigraphic horizons (SB1-SB6) into the grid (Fig. 14). Fig. 14 shows the maximum depth values for the Yuanyanggou and Qingshui Sag. The Huanxiling area is located in the south of the western gentle slope, and the Xinglongtai buried hill is adjacent to the north of the Qingshui Sag.

4.4.2. Facies model

The 3D facies model of the Western Depression was established by upscaling the lithofacies log of key wells—which contains sandstones (FDMs-W, FDM-E, SFMs, SLMs, SDLMs, and NSFMs)—using Sequential Indicator Simulation (SIS) method (Figs. 12 and 15). FDMs are deposited on the western gentle slope of every sequence, with the most significant volume percentages (24.27%) being found in SQ2. SFMs mainly occurred on the step fault zone and central sags of SQ3 and SQ5, with volume percentages of 20.06% and 7.18%, respectively. The volume of SDLMs increased between SQ2 (2.98%) and SQ4 (17.92%) periods. SLMs mostly formed in SQ2 (33.18%) during the initial rift stage. The occurrence of NSPMs is limited to the eastern steep slope with similar volume percentages ranging from 11.12% to 12.48%.

4.4.3. Geochemical properties model

The 3D property modeling incorporated models of several geochemical parameters (*TOC*, HI, and R_o) (Figs. 16, 18 and 19). The 3D *TOC* model shows an increasing trend from the slope toward the center of the lake (Fig. 16). The contour maps of average *TOC* values of mudstones for the four sequences are displayed in Fig. 17a–d. The average *TOC* contents of mudstones in SQ3 ranges from 0.5% to 2.5%, higher than the other sequences (Fig. 17d). The areal

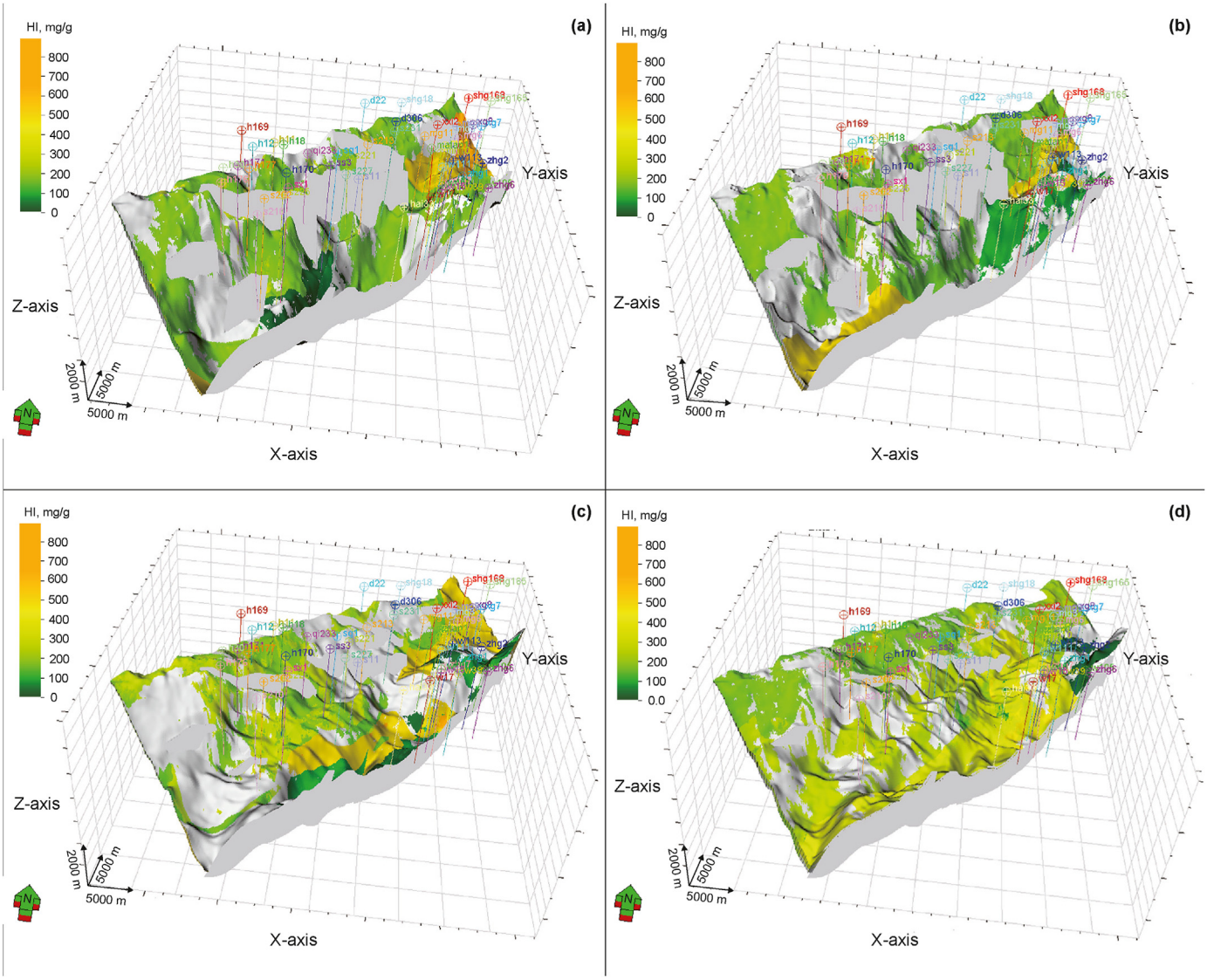

Fig. 18. HI model of the Shahejie Formation in the Western Depression; (a) SQ2, (b) SQ3, (c) SQ4, (d) SQ5.

distributions of average *TOC* contents in SQ2, SQ4, and SQ5 are similar, within the range of 0.5%–2.0% (Fig. 17a–d). The 3D HI model suggests that mainly mudstones containing type III organic matter were deposited on the eastern steep slope, as represented by the value HI < 150 mg/g. Mudstones containing type I-II$_2$ organic matter were mostly deposited on the western gentle slope (Fig. 18). The 3D R_o model was constructed from the three linear fitting equations representing the relationships between the R_o data and their corresponding depths for the northern, central, and southern parts of the study area (Fig. 19). It is concluded that the mudstones in the Qingshui and Yuanyanggou Sags have reached the late-mature stage, while mudstones in the western gentle slope are still in the mature stage (Fig. 19).

5. Discussion

5.1. Identification of effective gas source rocks

In the present work, we regard gas source rocks as rocks that have generated or are capable of producing natural gas. Previous studies have generally followed two main definitions of source rocks: rocks that have produced or are capable of producing oil; or rocks that have produced and expelled enough crude oil to form industrial accumulations (Hunt, 1981). The definition of gas source rocks in this study is referenced to Tissot's view because it does require that sets of gas source rocks be correlated to specific gas pools.

It is proposed that the effectiveness of gas source rocks can be determined by using a classification scheme that incorporates the nature of natural gas and the organic matter type of its related source rocks. The carbon isotopes of ethane and propane ($\delta^{13}C_2$ and $\delta^{13}C_3$) for thermogenic gas samples are commonly used to distinguish genetic types (Liu et al., 2019). The carbon isotope compositions of kerogens in gas source rocks are often ambiguous due to the heterogeneity of organic matter types within the same set of source rocks and limited data, which may lead to considerable errors in the conclusion of gas-source correlation (Dai, 1992; Liu et al., 2019).

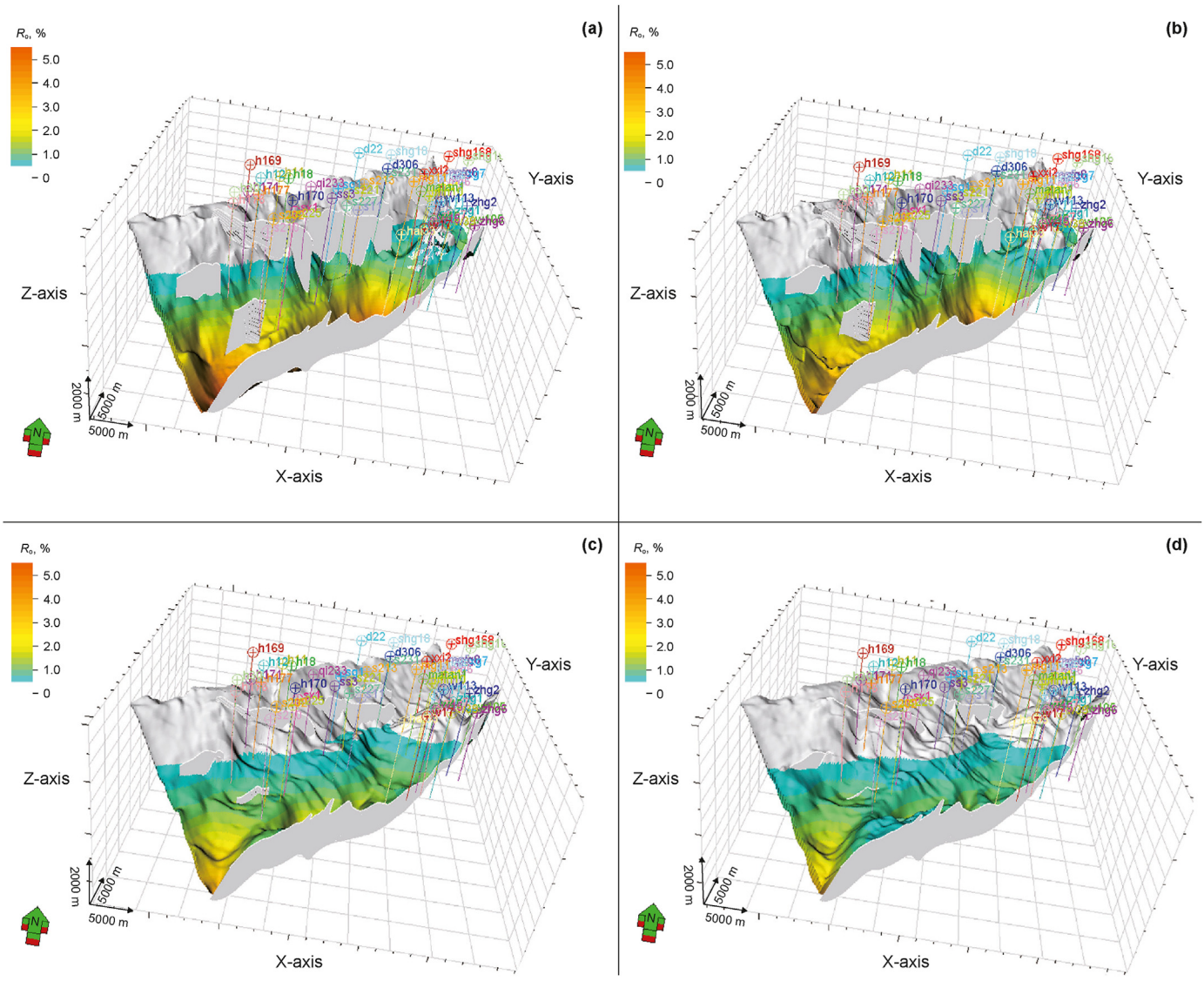

Fig. 19. R_o model of the Shahejie Formation in the Western Depression; (a) SQ2, (b) SQ3, (c) SQ4, (d) SQ5.

Table 1
Effective gas source rock identification criteria for the Western Depression.

Type of gas source rock	Limitation of effectiveness
Microbial source rock	Depth <2000 m, *TOC* > 1.25 %
Goal-type gas source rock	Type III kerogens, *TOC* >0.5 %
Oil-type gas source rock	Type I and II kerogens, *TOC* > 0.48%, R_o > 1.3%

Three types of natural gas have been distinguished in previous studies—coal-type, oil-type, and microbial—which are derived from humic organic matter in Mbr 3 of the Shahejie Fm, sapropelic organic matter in Mbrs 3 and 4 of the Shahejie Fm, and biodegraded crude oil, respectively (Huang et al., 2017; Wang et al., 2018; Pei et al., 2022). This study combines kerogen types, R_o values, and *TOC* contents to distinguish three types of effective gas source rocks corresponding to the three gas genesis types in the Western Depression (Table 1).

(1) Effective microbial gas source rocks produce natural gas through microbial activity, so the primary constraints are microbial survival conditions, including burial temperature (T < 75 °C) and nutrient supply (*TOC* > 1.25%) (Gao et al., 2011; Liu et al., 2019; X.N. Wang et al., 2022). Linear fitting between measured burial temperatures and depths in the Western Depression indicates a maximum burial depth for microbial source rocks of approximately 2000 m (Fig. 20).

(2) Effective coal-type gas source rocks produce natural gas from the threshold of hydrocarbon generation to the over-maturity stage (Welte and Tissot, 1984; Kotarba and Lewan, 2004; Wang et al., 2020). The lower cutoff of *TOC* content for the effectiveness of these source rocks is 0.5% (Peters, 1986).

(3) Effective oil-type gas source rocks contain type I-II kerogens and produce significant amounts of natural gas in the high to over maturity range (R_o >1.3 %) (Welte and Tissot, 1984). The lower cutoff of *TOC* content is 0.48%, following (Hou et al., 2021) for effective gas source rocks with lacustrine type II kerogen.

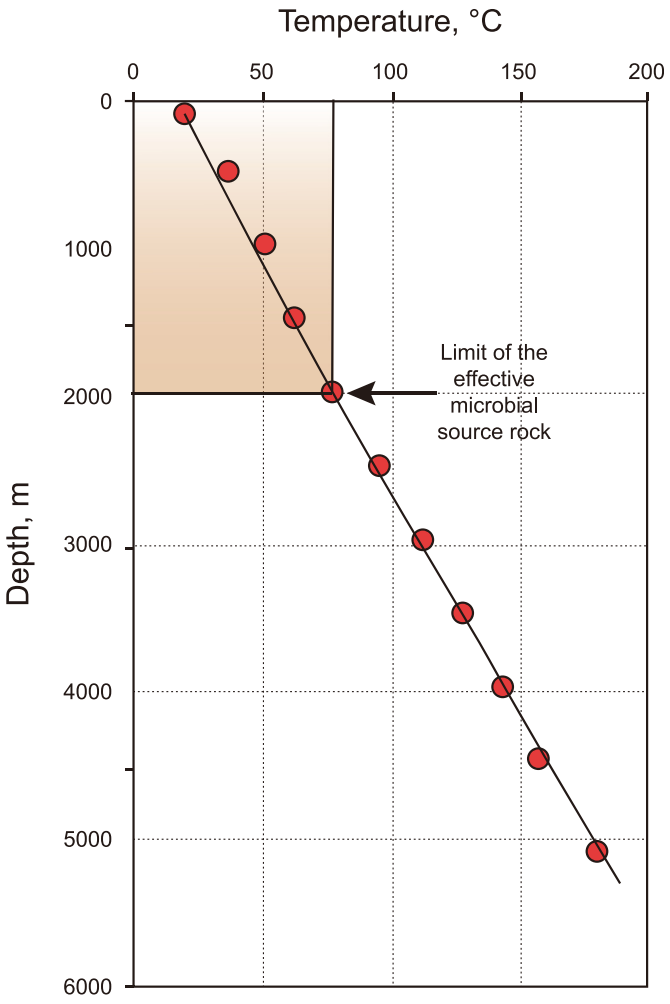

Fig. 20. Identification of the limit of effective gas source rocks.

5.2. Spatial distributions of effective gas source rocks

This study predicted the location of effective gas source rocks by constructing an effective gas source rocks model, filtered by combining the lithofacies model, geochemical parameters models, and criteria for effective gas source rocks. Microbial source rocks are widely dispersed on the western gentle slope, with the upper sequences having a broader distribution range than the lower due to their relatively shallower burial depths (Fig. 21). Oil-type gas source rocks containing sapropelic organic matter (type I and II kerogens), are mainly found in SQ2 and SQ3 in the central sags (Fig. 21a and b). Compared to other types, coal-type gas source rocks containing type III kerogens mostly occur in a restricted area (SQ3 and SQ4 of the northeastern steep slope zone), limited by narrow nearshore subaqueous fans (Fig. 21b and c). Overall, it can be concluded that oil-type, coal-type, and microbial effective gas source rocks are SLMs/SDLMs, NSFMs/FDMs-E, and FDMs-W, respectively.

Eight profiles were selected to display the spatial distributions of effective gas source rocks. The locations of these profiles are displayed in Fig. 22a. Lithofacies variation in the vertical source direction (southwest-northeast) is shown in profiles 1–4. Profile 1 lies in the shallow western slope zone, where microbial source rock formation development is primarily concentrated (Fig. 22b). Profile 2 is within the slope fracture belt, where only the lower sequences (SQ2 and SQ3) have developed effective gas source rocks because of the shallow burial depths (Fig. 22c). Profiles 3 and 4 lie in the center and eastern parts of depression and represent the main areas of effective gas source rock deposition (Fig. 22d and e). Profiles 5 to 8 show the major provenance direction (northwest-southeast), the oil-type gas source rocks mainly occur in the southwest part of the study area (Fig. 22f). In contrast, coal-type gas source rocks primarily occur in the northeast part (Fig. 22i). In summary, a strong correlation is found between sedimentary facies and effective source rock types, which the scale of fan deltas may constrain and the transport distance of the terrestrial organic matter (Figs. 13 and 22).

5.3. Effective gas source rock volume

This work quantitatively calculated each category of effective gas source rocks in every sequence by counting the number of grids in the effective gas source rock model (Table 2). The bar chart shows a survey of effective gas source rock volumes in four sequences in the Western Depression (Fig. 23). The bar chart compares the volumes of the three types of effective source rocks in each sequence, which shows that the largest volume of effective gas source rocks is to be found in SQ4, and the least in SQ5 (Fig. 23). The pie charts show the volume of mudstones in each sequence, with the data divided into four areas (cap rocks; effective microbial gas source rocks, oil-type gas source rocks, and coal-type gas source rocks) (Fig. 24). The percentage for cap rocks made around half the total in SQ2-SQ4 (45.01%, 53.89%, and 44.11%, respectively) but over half of the total in SQ5 (70.76%). The volumes of effective coal- and oil-type gas source rocks are comparable in SQ2 and SQ4, over 20%, but effective microbial gas source rocks are almost half this value, around 10%. The percentage of effective coal-type gas source rocks is largest in SQ3 (25.22%) and smallest in SQ5 (5.87%) (Fig. 24). In general, SQ2-SQ5 are all potential gas source formations, with the largest effective gas source rock volume being found ins SQ4, followed by SQ3.

5.4. Implication for gas exploration

The locations of the natural gas reservoir types in the Western Depression correlate well with the predicted sites of the different kinds of effective gas source rocks. Previous studies have shown that the natural gas in the Xinglongtai block is mainly coal-type gas and that the distribution of gas pools is consistent with the locations of coal-type effective source rocks in the steep slope. The Huangxiling gas reservoir hosts mainly oil-type gas, consistent with the area of oil-type gas source rocks in the central sags (Huang et al., 2017; Wang et al., 2018; Pei et al., 2022). Few proven gas reserves in the central sags and southern part of the steep slope are also explored, but a certain volume of effective coal-type and oil-type gas source rocks was identified in this area, which might therefore have potential as an exploration field. However, the gas-source correlation needs to be further verified and more precise calculations made to quantify the hydrocarbon source rocks accurately.

Previous studies indicate that key to evaluating natural gas resource potential and pinpointing optimal exploration areas is accurately identifying the genetic types and sources of natural gas. (Liu et al., 2019). However, it is necessary to accurately locate effective gas source rocks for discovering deep or in-source natural gas reservoirs. This paper makes a case for using 3D geological modeling techniques to accomplish this objective by quantitatively assessing the effective gas source rocks using a combination of geochemical parameters, seismic, well logging, and other geological data, particularly in areas and formations where is a lack of wells and samples. The classification of the gas source rock and the

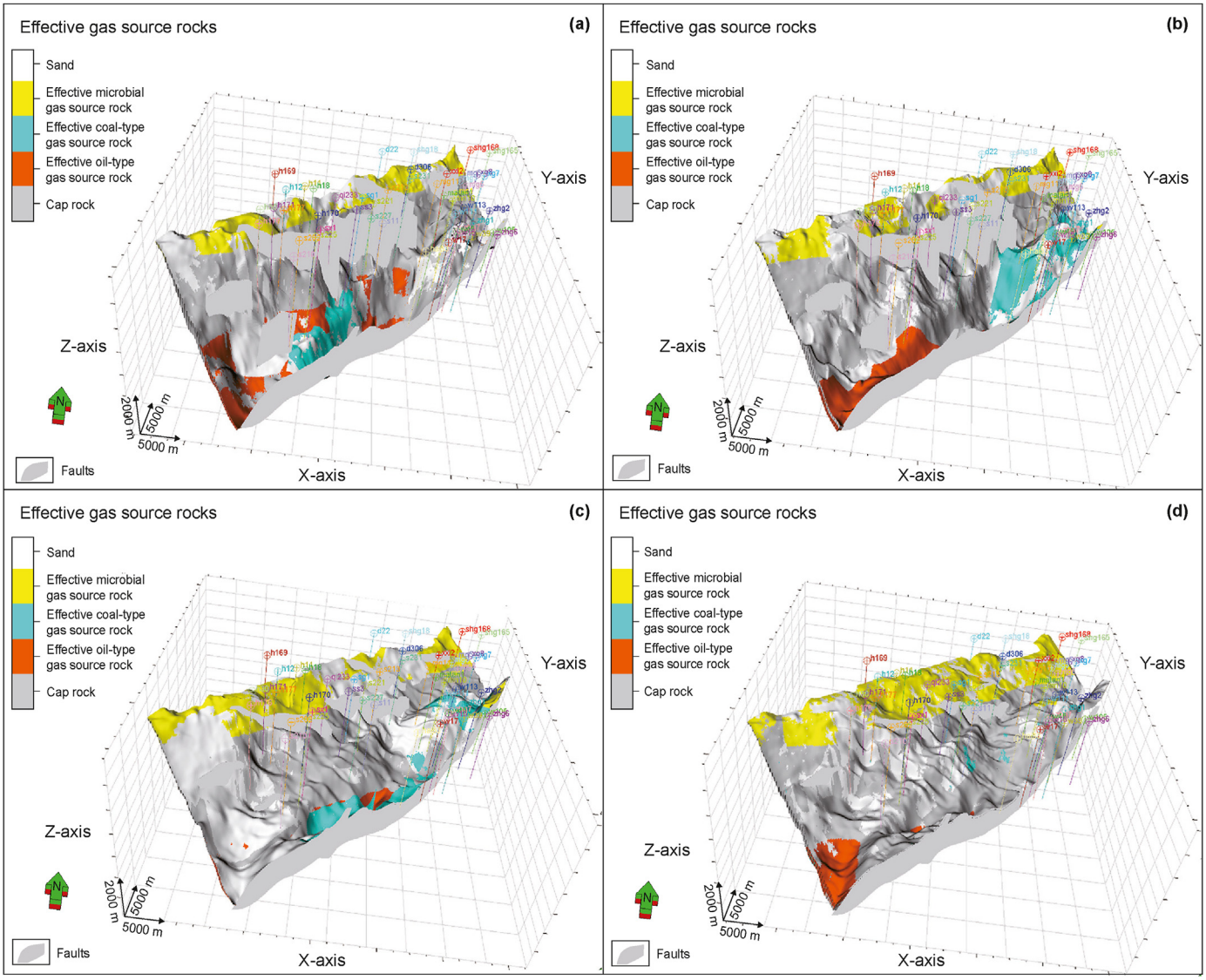

Fig. 21. Effective gas source rock model of the Shahejie Formation in Western Depression; (a) SQ2, (b) SQ3, (c) SQ4, (d) SQ5.

spatial distribution forecast method employed in this work provides a sound geological basis for gas-source correlation. The proposed method hinges on subdividing mudstone types according to sedimentary facies, and harnesses the evolution and distribution of these facies to constrain the three-dimensional modeling of mudstones and their organic geochemical characteristics. This approach ensures a more accurate and granular distribution of source rocks, aligning with the heterogeneous distribution requirements of gas source rocks. Furthermore, extending three-dimensional geological modeling to hydrocarbon source layers constitutes a significant advancement in this field. Consequently, this method offers theoretical support for further natural gas resource estimations and the identification of promising exploration areas, providing a universally applicable and practical methodology for investigating gas source rocks in lacustrine basins.

6. Conclusion

Identifying and quantifying effective source rocks is pivotal in establishing oil and gas exploration targets and optimizing well placement. Natural gas can originate from various sources, each corresponding to distinct stages of gas generation. This diversity can render the identification and classification of effective source rocks challenging due to the absence of unified criteria. In our study, we introduce a method for categorizing source rocks into three classes: microbial, coal, and oil-type source rocks. For each source rock category, we determine the minimum effectiveness threshold based on organic geochemical characteristics such as the abundance, type, and maturity of organic matter.

A precise characterization of the three types of effective source rocks requires detailed understanding of the traits and distribution of mudstones, along with their geochemical properties. Our geochemical analysis reveals that within each sequence stratigraphic unit, both the *TOC* content and HI of source rocks normally distribute across various sedimentary facies. This suggests a robust correlation between sedimentary facies and geochemical properties. We introduce a three-dimensional modeling method to predict effective source rocks, incorporating facies-controlled

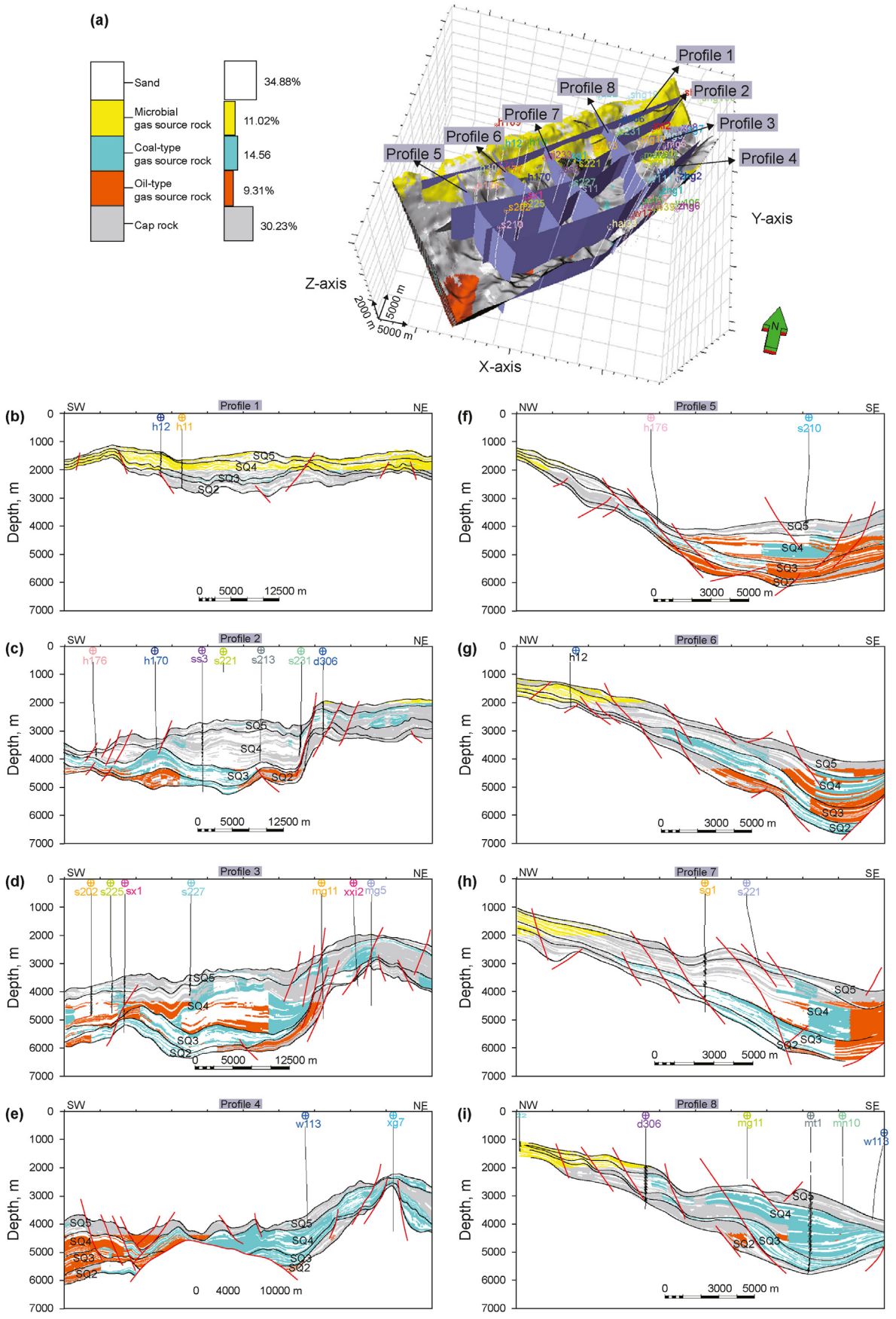

Fig. 22. Eight cross-sections were extracted from the 3D effective gas source rock model; (a) location of the eight profiles; (b)–(e) four profiles of the major provenance direction; (f)–(i) four profiles of the vertical provenance direction.

Table 2
Efficient gas source rock volume.

3rd sequence	Volume, km^3					
	Bulk	Mudstones	Effective gas source rock	Effective microbial gas source rock	Effective coal-type gas source rock	Effective Oil-type gas source rock
SQ2	298.5	180.9	99.5	21.2	41.2	37.1
SQ3	370.2	351.4	162.0	18.3	88.6	55.1
SQ4	855.3	442.5	247.3	43.1	94.7	109.5
SQ5	372.6	265.2	77.6	30.8	15.6	31.2
Total	1896.6	1240	586.4	113.4	240.1	232.9

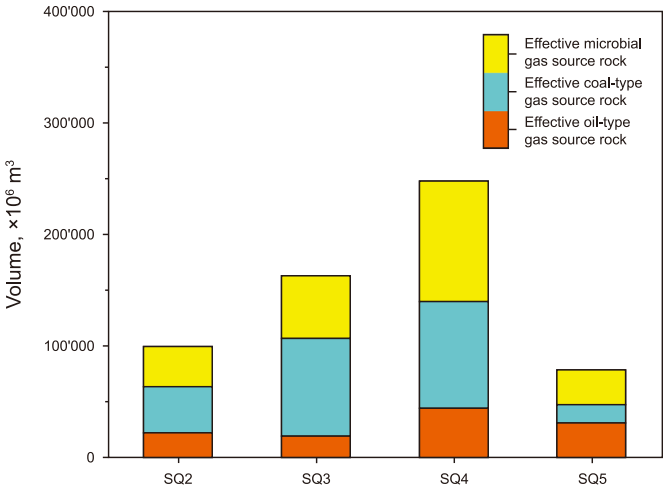

Fig. 23. Volume of different effective gas source rocks in each sequence.

modeling to guide the estimation of lithology and geochemical parameters.

A 3D effective gas source rocks model was established for the Shahejie Fm in the Western Depression of the Liaohe Subbasin. This model calculated that the total volume of effective gas source rocks is 586.3 km^3, comprised of effective microbial, oil-type, and coal-type gas source rocks (113.4 km^3, 232.9 km^3, and 240.1 km^3, respectively). SQ2 to SQ4 in the Shahejie Fm are the major gas-generating intervals, and the central sag might prove to be a favorable area for gas exploration. This approach represents a practical and novel method for investigating gas source rock that can be effectively utilized to direct exploration.

Declaration of competing interest

The authors declare that they have no known competing financial interests or personal relationships that could have appeared to influence the work reported in this paper.

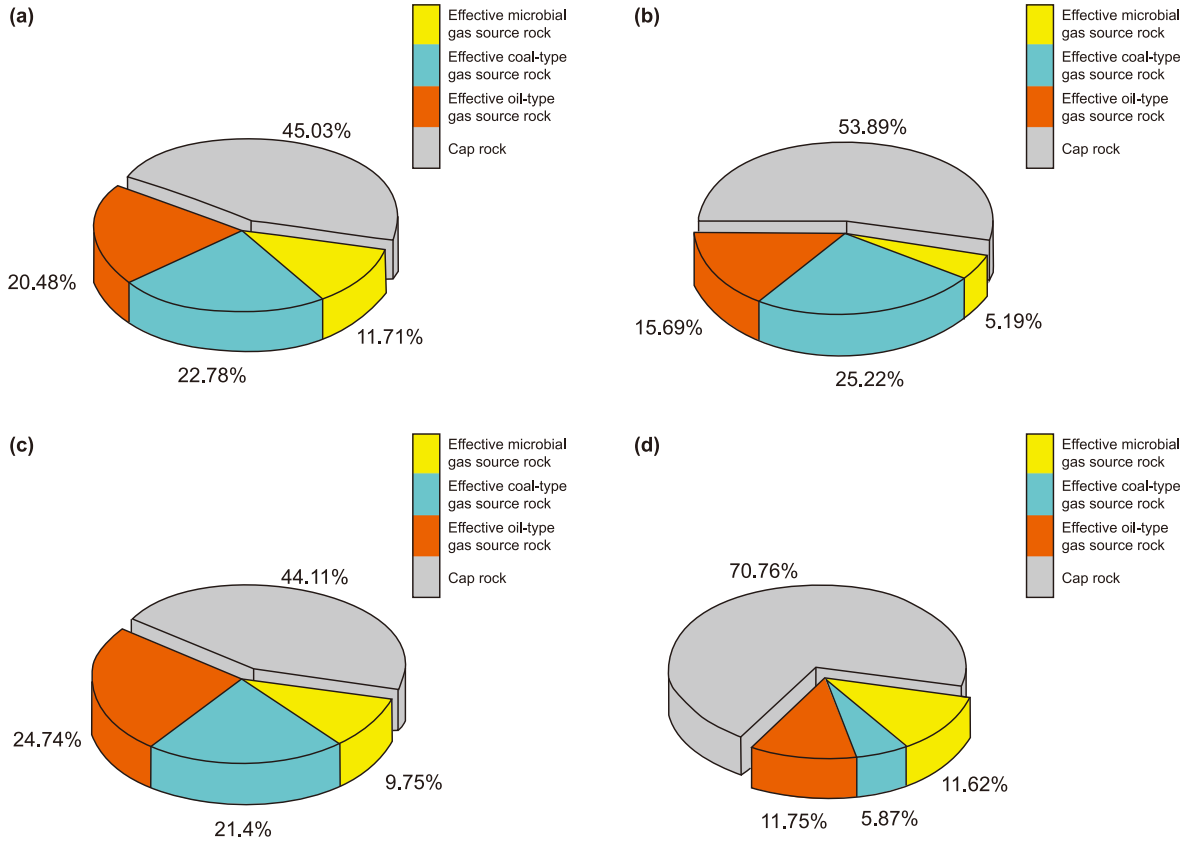

Fig. 24. Relative contribution of effective gas source rocks for each stratum; (a) SQ2, (b) SQ3, (c) SQ4, (d) SQ5.

Acknowledgment

The authors would like to thank CNPC Liaohe Oilfield Exploration Company for data support, for making an academic license available for the use of Petrel, and for helpful discussions on the topics addressed in this work.

Appendix A. Supplementary data

Supplementary data to this article can be found online at https://doi.org/10.1016/j.petsci.2024.03.007.

References

Ali, A.M., Radwan, A.E., Abd El-Gawad, E.A., Abdel-Latief, A.A., 2022. 3D integrated structural, facies and petrophysical static modeling approach for complex sandstone reservoirs: a case study from the coniacian–santonian matulla formation, july Oilfield, gulf of suez, Egypt. Nat. Resour. Res. 31, 385–413. https://doi.org/10.1007/s11053-021-09980-9.

Al-Mudhafar, W.J., 2017. Multiple-Point Geostatistical Lithofacies Simulation of Fluvial Sand-Rich Depositional Environment: A Case Study from Zubair Formation/South Rumaila Oil Field. SPE Reservoir Evaluation & Engineering. https://doi.org/10.2118/187949-PA.

Alabert, F.G., Massonnat, G.J., 1990. Heterogeneity in a complex turbiditic reservoir: stochastic modelling of facies and petrophysical variability. In: SPE Annual Technical Conference and Exhibition. https://doi.org/10.2118/20604-MS.OnePetro.

Anas, M.M., Scott, K.A., Wissel, B., 2015. Carbon budgets of boreal lakes: state of knowledge, challenges, and implications. Environ. Rev. 23, 275–287. https://doi.org/10.1139/er-2014-0074.

Anees, A., Zhang, H.C., Ashraf, U., Wang, R., Liu, K., Abbas, A., Ullah, Z., Zhang, X.N., Duan, L.Z., Liu, F.W., 2022. Sedimentary facies controls for reservoir quality prediction of lower shihezi member-1 of the Hangjinqi area, Ordos Basin. Minerals 12, 126. https://doi.org/10.3390/min12020126.

Azevedo, L., Soares, A., 2017. Geostatistical Methods for Reservoir Geophysics. Springer, Berlin.

Behar, F., Beaumont, V., Penteado, H.D.B., 2001. Rock-Eval 6 technology: performances and developments. Oil Gas Sci. Technol. 56, 111–134. https://doi.org/10.2516/ogst:2001013.

Bordenave, M., Espitalié, J., Leplat, P., Oudin, J., Vandenbroucke, M., 1993. Screening Techniques for Source Rock Evaluation. Applied petroleum geochemistry, France, pp. 217–278.

Cannon, S., 2018. Reservoir Modelling: A Practical Guide. John Wiley & Sons, UK.

Dai, J.X., 1992. Identification of various alkane gases. Sci. Sin. 185–193 (in Chinese).

Dai, J.X., 1993. Identification of Coal-Formed Gas and Oil-type Gas by Light Hydrocarbon. Petroleum Exploration and Development, pp. 26–32. https://CNKI:SUN:SKYK.0.1993-05-003 (in Chinese).

Dai, J.X., Xia, X., Zhao, L., Hong, F., 1998. Characteristics of Helium Isotope Composition in Bohai Bay Basin and Ordos Basin and its Significance for Gas Bearing, pp. 402–408 (in Chinese).

Damsleth, E., Tjolsen, C.B., Omre, H., Haldorsen, H.H., 1992. A two-stage stochastic model applied to a North Sea reservoir. J. Petrol. Technol. 44, 402–486. https://doi.org/10.2118/20605-PA.

Dembicki, H.J., 2009. Three common source rock evaluation errors made by geologists during prospect or play appraisals. AAPG (Am. Assoc. Pet. Geol.) Bull. 93, 341–356. http://10.1306/10230808076.

Faramawy, S., Zaki, T., Sakr, A.A.E., 2016. Natural gas origin, composition, and processing: a review. J. Nat. Gas Sci. Eng. 34, 34–54. https://doi.org/10.1016/j.jngse.2016.06.030.

Feng, Y.L., Jiang, S., Hu, S.Y., Li, S.T., Lin, C.S., Xie, X., 2016. Sequence stratigraphy and importance of syndepositional structural slope-break for architecture of Paleogene syn-rift lacustrine strata, Bohai Bay Basin, E. China. Mar. Petrol. Geol. 69, 183–204. https://doi.org/10.1016/j.marpetgeo.2015.10.013.

Gao, Y., Jiang, X.L., Liu, F., Wang, X.Y., Liu, R.H., 2017. Sedimentary characteristics and formation mechanisms of lacustrine beach-bars in the fourth member of the Shahejie Formation in the Shubei area, western depression of the Liaohe Oilfield, China. J. Earth Sci. 28, 1178–1190. https://doi.org/10.1007/s12583-016-0928-0.

Gao, Y., Jin, Q., Shuai, Y.H., Wang, H., 2011. Genetic types and accumulation conditions of biogas in Bohaiwan Basin. Nat. Gas Geosci. 22, 407–414. https://10.1002/9781444350302.wbhe1011 (in Chinese).

Hou, L.H., Huang, H.P., Yang, C., Ma, W.J., 2021. Experimental simulation of hydrocarbon expulsion in semi-open systems from variable organic richness source rocks. ACS Omega 6, 14664–14676. https://doi.org/10.1021/acsomega.1c01800.

Hu, L.G., Fuhrmann, A., Poelchau, H.S., Horsfield, B., Zhang, Z.W., Wu, T.S., Chen, Y.X., Li, J.Y., 2005. Numerical simulation of petroleum generation and migration in the Qingshui sag, western depression of the Liaohe basin, northeast China. AAPG (Am. Assoc. Pet. Geol.) Bull. 89, 1629–1649. https://doi.org/10.1306/07280504069.

Hu, S.B., O'Sullivan, P.B., Raza, A., Kohn, B.P., 2001. Thermal history and tectonic subsidence of the Bohai Basin, northern China: a Cenozoic rifted and local pull-apart basin. Phys. Earth Planet. In. 126, 221–235. https://doi.org/10.1016/S0031-9201(01)00257-6.

Huang, S.P., Feng, Z.Q., Gu, T., Gong, D.Y., Peng, W.L., Yuan, M., 2017. Multiple origins of the Paleogene natural gases and effects of secondary alteration in Liaohe Basin, northeast China: insights from the molecular and stable isotopic compositions. Int. J. Coal Geol. 172, 134–148. https://doi.org/10.1016/j.coal.2017.01.009.

Hunt, J.M., 1981. Source rock charicterization by thermal distillation and pyrolisis. In: Atkinson, G., Zuckerman, J.J. (Eds.), Origin and Chemistry of Petroleum. Pergamon, pp. 57–65. https://doi.org/10.1016/B978-0-08-026179-9.50007-4.

Khattab, M.A., Radwan, A.E., El-Anbaawy, M.I., Mansour, M.H., El-Tehiwy, A.A., 2023. Three-dimensional structural modelling of structurally complex hydrocarbon reservoir in October Oil Field, Gulf of Suez, Egypt. Geol. J. https://doi.org/10.1002/gj.4748.

Kotarba, M.J., Lewan, M.D., 2004. Characterizing thermogenic coalbed gas from Polish coals of different ranks by hydrous pyrolysis. Org. Geochem. 35, 615–646. https://doi.org/10.1016/j.orggeochem.2003.12.001.

Lai, H.F., Li, M.J., Jian, X.L., Wang, L., Liu, J., Wang, G.Y., Liu, P., Dai, J.H., 2020a. An integrated sequence stratigraphic–geochemical investigation of the Jurassic source rocks in the North Yellow Sea Basin, eastern China. AAPG (Am. Assoc. Pet. Geol.) Bull. 104, 2145–2171. https://doi.org/10.1306/05212019072.

Lai, H.F., Li, M.J., Mao, F.J., Liu, J.G., Xiao, H., Tang, Y.J., Shi, S.B., 2020b. Source rock types, distribution and their hydrocarbon generative potential within the Paleogene Sokor-1 and LV formations in Termit Basin, Niger. Energy Explor. Exploit. 38, 2143–2168. http://10.1177/0144598720915534.

Lai, W.Z., 2000. Gas Exploration Potential in Bohai Sea. China Offshore Oil Gas 25–30 (in Chinese).

Li, D.S., 1981. Geological structure and Hydrocarbon occurrence of Bohai gulf oil and gas basin. Marine Geol. Res. 3–20 (in Chinese). https://10.16562/j.cnki.0256-1492.1981.01.002.

Li, M.J., Simoneit, B.R.T., Zhong, N.N., Fang, R.H., 2013. The distribution and origin of dimethyldibenzothiophenes in sediment extracts from the Liaohe Basin, East China. Org. Geochem. 65, 63–73. https://10.1016/j.orggeochem.2013.10.007.

Li, X.G., 2020. Accumulation conditions and key exploration & development technologies of heavy oil in Huanxiling oilfield in Liaohe depression, Bohai Bay Basin. Petroleum Res. 5, 18–38. https://doi.org/10.1016/j.ptlrs.2020.01.004.

Liu, Q.Y., Wu, X.Q., Wang, X.F., Jin, Z.J., Zhu, D.Y., Meng, Q.Q., Huang, S.P., Liu, J.Y., Fu, Q., 2019. Carbon and hydrogen isotopes of methane, ethane, and propane: a review of genetic identification of natural gas. Earth Sci. Rev. 190, 247–272. https://doi.org/10.1016/j.earscirev.2018.11.017.

Mu, G.Y., Zhong, N.N., Liu, B., Yu, T.C., Liu, Y., 2010. The quantitative evaluation method of lacustrine mudstone source rock and its application. Acta Pet. Sin. 31, 218–224+230. https://10.7623/syxb201002007 (in Chinese).

Passey, Q.R., Bohacs, K., Esch, W.L., Klimentidis, R., Sinha, S., 2010. From oil-prone source rock to gas-producing shale reservoir–geologic and petrophysical characterization of unconventional shale-gas reservoirs. International Oil and Gas Conference and Exhibition in China. https://doi.org/10.2118/131350-MS. OnePetro.

Pei, L.X., Wang, X.F., Gao, G., Liu, W.H., 2022. Geochemical heterogeneity, origin and secondary alteration of natural gas inside and outside buried hills of Xinglongtai area, West Sag, Liaohe Depression, Bohai Bay Basin. J. Petrol. Sci. Eng. 208, 109456. https://doi.org/10.1016/j.petrol.2021.109456.

Peters, K.E., 1986. Guidelines for evaluating petroleum source rock using programmed pyrolysis. AAPG (Am. Assoc. Pet. Geol.) Bull. 70, 318–329. https://doi.org/10.1306/94885688-1704-11D7-8645000102C1865D.

Peters, K.E., Cassa, M.R., 1994. Applied source rock geochemistry: chapter 5: Part II. Essential Elements in the Petroleum System–From Source to Trap. AAPG, US, pp. 93–120.

Qi, J.F., Yang, Q., 2010. Cenozoic structural deformation and dynamic processes of the Bohai Bay basin province, China. Mar. Petrol. Geol. 27, 757–771. https://doi.org/10.1016/j.marpetgeo.2009.08.012.

Sahoo, T.R., Funnell, R.H., Brennan, S.W., Sykes, R., Thrasher, G.P., Adam, L., Lawrence, M.J.F., Kellett, R.L., Ma, X., 2021. Delineation of coaly source rock distribution and prediction of organic richness from integrated analysis of seismic and well data. Mar. Petrol. Geol. 125, 104873. https://doi.org/10.1016/j.marpetgeo.2020.104873.

Speight, J.G., 2022. Gas Engineering. De Gruyter, Berlin.

Wang, J.Y., Wang, J.A., Xiong, L.P., Zhang, J.M., 1985. Analysis of factors affecting heat flow density determination in the Liaohe Basin, North China. Tectonophysics 121, 63–78. https://doi.org/10.1016/0040-1951(85)90268-9.

Wang, Q.C., Bao, Z.D., He, P., 2010. Sequence stratigraphic responses to the lacustrine basin deep-faulted period in the north area of the western sag Liaohe Depression. Petrol. Explor. Dev. 37, 11–20. https://JournalArticle/5af5b9abc095d718d8287b27 (in Chinese).

Wang, Q., Hao, F., Niu, C.M., Zou, H.Y., Miao, Q.Y., Yin, J., Cao, Y.J., Liu, M.X., 2021. Origins and deep petroleum dynamic accumulation in the southwest part of the Bozhong depression, Bohai Bay Basin: insights from geochemical and geological evidences. Mar. Petrol. Geol. 134, 105347. https://doi.org/10.1016/j.marpetgeo.2021.105347.

Wang, W.Y., Pang, X.Q., Chen, Z.X., Chen, D.X., Ma, X.H., Zhu, W.P., Zheng, T.Y., Wu, K.L., Zhang, K., Ma, K.Y., 2020. Improved methods for determining effective sandstone reservoirs and evaluating hydrocarbon enrichment in petroliferous basins. Appl. Energy 261, 114457. https://doi.org/10.1016/j.petrol.2020.107843.

Wang, W.Y., Pang, X.Q., Wang, Y.P., Chen, Z.X., Li, C.R., Ma, X.H., 2022. Hydrocarbon

expulsion model and resource potential evaluation of high-maturity marine source rocks in deep basins: example from the Ediacaran microbial dolomite in the Sichuan Basin, China. Petrol. Sci. 19, 2618–2630. https://doi.org/10.1016/j.petsci.2022.11.018.

Wang, X.B., Jiang, Z.X., Hu, G.Y., Fan, E.T., Wang, J.H., Lu, H., 2019. Sendimentary facies and evolusion of upper fourth member of paleogene shahejie formation in western sag of Liaohe Basin. J. Jilin Univ. (Earth Sci. Ed.) 49, 1222–1234 (in Chinese). http://10.13278/j.cnki.jjuese.20180054.

Wang, X.N., Li, J.R., Jiang W, Q., Zhang, H., Feng, Y.L., Yang, Z., 2022. Characteristics, current exploration practices, and prospects of continental shale oil in China. Adv. Geo-Energy Res. 6, 454–459. https://doi.org/10.1016/j.apenergy.2019.114457.

Wang, Y.S., Hu, Y.J., Huang, S.Q., Kang, W.J., Chen, Y.C., 2018. Geological conditions, petential and exploration direction of nature gas in Liaohe Depression, Bohai by Basin. Nutrual Gas Geosci. 29, 1422–1432 (in Chinese).

Welte, D., Tissot, P., 1984. Petroleum Formation and Occurrence. Springer, German.

Xie, Y.H., Zhu, X.M., Zhao, K., 2010. Sequence-stratigraphic framework on paleogene of the Liaohe western depression. Sci. Technol. Rev. 28, 58–64 (in Chinese).

Xu, C.G., Yu, H.B., Wang, J., Liu, X.J., 2019. Formation conditions and accumulation characteristics of Bozhong 19-6 large condensate gas field in offshore Bohai Bay Basin. Petrol. Explor. Dev. 46, 27–40. https://doi.org/10.1016/S1876-3804(19)30003-5.

Xu, Z.J., Wang, Y., Jiang, S., Fang, C., Liu, L.F., Wu, K.J., Luo, Q., Li, X., Chen, Y.Y., 2022. Impact of input, preservation and dilution on organic matter enrichment in lacustrine rift basin: a case study of lacustrine shale in Dehui Depression of Songliao Basin, NE China. Mar. Petrol. Geol. 135, 105386. https://doi.org/10.1016/j.marpetgeo.2021.105386.

Yang, S.B., Li, M., Liu, J., X, Q., Han, Q.Y., Wu, J., Zhong, N.N., 2019. Thermodynamic stability of methyldibenzothiophenes in sedimentary rock extracts: based on molecular simulation and geochemical data. Org. Geochem. 129, 24–41. https://doi.org/10.1016/j.orggeochem.2018.10.012.

Yang, Z., Zou, C.N., 2019. "Exploring petroleum inside source kitchen": connotation and prospects of source rock oil and gas. Petrol. Explor. Dev. 46, 181–193. https://doi.org/10.1016/S1876-3804(19)30018-7.

Zeng, B., Li, M.J., Wang, X., Wang, F.Z., Gong, C.L., Lai, J., Shi, Y., 2022. Source rock evaluation within a sequence stratigraphic framework of the palaeogene liushagang Formation in the fushan depression, south China sea. Geol. J. https://doi.org/10.1002/gj.4419.

Zeng, B., Li, M.J., Zhu, J.Q., Wang, X., Shi, Y., Zhu, Z.L., Guo, H., Wang, F.Z., 2021. Selective methods of TOC content estimation for organic-rich interbedded mudstone source rocks. J. Nat. Gas Sci. Eng. 93, 104064. https://doi.org/10.1016/j.jngse.2021.104064.

Zhang, S.J., Shao, L.Y., Jie, S., Liu, D.T., Chen, G.S., Ren, C.L., 2008. Application of facies-controlled modeling technology to the fault-block A11 in A'nan Oilfield. Petrol. Explor. Dev. 35, 355–361. https://doi.org/10.1016/S1876-3804(08)60083-X.

Zhu, C.Z., Gang, W.Z., Li, X.F., Wang, N., Guo, Y., Zhao, X.Z., Wang, Y.F., Pu, X.G., 2022. The sorting effect of hydrodynamics on the geochemical compositions of sedimentary organic matter in a lacustrine rift basin: significance for hydrocarbon exploration on the Qibei slope, Bohai Bay Basin, China. Mar. Petrol. Geol. 141, 105705. https://doi.org/10.1016/j.marpetgeo.2022.105705.